


## Spectra of supersaturation and liquid water content in cloud turbulence

Toshiyuki Gotoh <sup>1,2,\*</sup>, Izumi Saito <sup>1</sup> and Takeshi Watanabe<sup>1</sup><sup>1</sup>*Department of Physical Science and Engineering, Nagoya Institute of Technology,  
Gokiso, Nagoya, 466-8555, Japan*<sup>2</sup>*Research and Education Center for Natural Sciences, Keio University,  
Hiyoshi, Yokohama, 223-8521, Japan*

(Received 4 July 2021; accepted 2 November 2021; published 30 November 2021)

Spectra of supersaturation and liquid water content (LWC) fluctuations in cloud turbulence are theoretically studied. Equations for the variance spectra are derived using the Lagrangian renormalized approximation and examined through asymptotic analysis. Our results show that the wave-number-dependent Damköhler number, defined as the ratio of the turbulent eddy turnover time to the phase relaxation time of the supersaturation, controls the scalar transfer functions and the supersaturation excitation by turbulence. Additionally, the supersaturation spectrum  $E_s(k)$  has three power-law ranges. Here two ranges follow  $k^{-5/3}$ ; however, their amplitudes differ depending on the large-scale Damköhler number and the input ratio of the supersaturation excitations in the associated range. The third range of  $E_s(k) \propto k^{-1-2C_b D_K}$  includes  $C_b$  and  $D_K$  representing the Batchelor constant and Damköhler number corresponding to the Kolmogorov time, respectively. The LWC spectrum  $E_\phi(k)$  reveals two power-law ranges:  $k^{-5/3}$  for  $k < k_{\phi*}$  and  $k^{-1}$  for  $k_{\phi*} < k$ , in which the transition wave number  $k_{\phi*}\bar{\eta}$  is given by the input ratio of the supersaturation excitations in the two  $k^{-5/3}$  ranges by the turbulence and is consistent with field measurement results.

DOI: [10.1103/PhysRevFluids.6.110512](https://doi.org/10.1103/PhysRevFluids.6.110512)

## I. INTRODUCTION

Recent developments in the measurement of cloud properties has allowed for the accumulation of a considerable amount of cloud microphysics data, gathered by various means including airplanes [1–5], high-elevation measurements [6], and cloud kites [7]. The power spectrum of liquid water content (LWC), in particular, has attracted much interest [1,2,6,8–11]. The LWC spectrum is  $k^{-5/3}$  at low wave numbers but trends toward  $k^{-1}$  at 2–5 m, which corresponds to  $k\bar{\eta} \approx 0.002$ , where  $\bar{\eta}$  is the Kolmogorov length [1,9]. High-elevation measurements from a mountain top have indicated an LWC power spectrum of  $f^{-5/3}$  for low frequencies; however, the spectrum is shallower and shows a transition at around 3 Hz (Fig. 12 of Siebert *et al.* [6]), corresponding to  $k\bar{\eta} \approx 0.0018$ . Notably, this transition occurs at wave-number values well inside the inertial-convective range. These findings lead to questions as to whether the observed  $k^{-1}$  spectrum is the Batchelor spectrum for a high Schmidt number [12], as well as why the transition wave number is so low compared to the theoretical condition of  $k\bar{\eta} \gg 1$ .

Much effort has been directed towards clarifying these observations. Among the arguments posed it is considered that the observed spectrum reflects actual physical phenomena and is not due to sampling error, and that the intermittency of the LWC is irrelevant for the spectrum which is the second order moment, but tends to manifest in high-order moments [13,14]. Mazin [8] argued

\*gotoh.toshiyuki@nitech.ac.jp

the effects of the phase relaxation time  $\tau_p$  to LWC fluctuations in turbulence. When  $\tau_p \gg \tau_{\text{turb}}$ , a significant phase change cannot take place; in this case, the LWC is just a passive scalar. However, when  $\tau_p \ll \tau_{\text{turb}}$ , the supersaturation responds quickly to the ambient turbulent field and attains a statistically steady state. In both cases, the LWC spectrum obeys  $k^{-5/3}$  scaling. On the other hand, when  $\tau_p \approx \tau_{\text{turb}}$ , the dynamics of the scalar transfer changes and the  $k^{-5/3}$  spectrum is modified, and the deviation of the LWC spectrum can be interpreted as the transition from one  $k^{-5/3}$  to another  $k^{-5/3}$  spectrum. However, how the two spectra match in the wave-number space is not debated. Jefferey [10] (see also [9,11]) examined the LWC spectrum enhancement at high wave numbers for rapidly changing random velocity (Kraichnan model [15–17]). A passive scalar such as the LWC is assumed to be excited by condensation-evaporation, which originates from the axisymmetric vertical structure of the mean field depending on the vertical coordinate and the vertical turbulent velocity. The result is an enhanced LWC spectrum, and the transition from  $k^{-5/3}$  to  $k^{-1}$  is found to occur at the wave numbers as seen in the observations. However, in the authors' view, it is questionable that the anisotropy at scales where the  $k^{-1}$  spectrum is observed leads to such a large enhancement of the LWC spectrum. And use of the random velocity which is delta correlated in time masks the role of the phase relaxation of the supersaturation relative to the turbulent mixing time that depends on scale.

In previous studies, the LWC fluctuations have been examined with respect to the measured LWC spectrum; however, supersaturation has not been considered. Given that supersaturation is responsible for the growth or decay of cloud droplets through the condensation-evaporation process, arguments that do not include analysis of supersaturation effects may lack the essential physics necessary to explain the LWC spectrum. Thus, the problem regarding LWC spectrum modification has yet to be resolved.

The purpose of the present paper is to answer the questions proposed and to gain insight into the spectral dynamics of the LWC and supersaturation variances over the entire range of the wave number. For this purpose, first, by taking a closer look at LWC and supersaturation from the microscopic viewpoint, we derive the fundamental and simple equations to the problem which allow theoretical analysis. Second, by using direct numerical simulations (DNSs) and the statistical theory of turbulence, we study the scaling of the supersaturation and LWC variance spectra. We stress also a viewpoint that spectral dynamics of scalar in turbulence which has its inherent characteristic time, such as the phase relaxation time that is independent of scale, poses a new type of the problem in the turbulent mixing. It is interesting and important to the physics of turbulence to study where the scaling behavior of the scalar fluctuations is broken and how the spectrum is modified.

The remainder of this paper is organized as follows. In Sec. II the Batchelor theory is reviewed as it plays a key role in the analysis, and we examine its performance by comparing the theory with DNS data. Section III presents the derivations of the governing equations for supersaturation and LWC. In Sec. IV the equations for the spectra of the supersaturation and LWC variances are derived. An asymptotic analysis of the spectra and the results are presented in Sec. V for the supersaturation and in Sec. VI for the LWC. Section VII provides a discussion of the results, and Sec. VIII summarizes our findings.

## II. BATCHELOR'S THEORY

In this section Batchelor's theory of mixing of passive scalar with a high Schmidt number,  $Sc = \nu/\kappa$ , is reviewed [12]. These ideas are classical, but their understanding is essential to appreciate the results on cloud turbulence in the following sections, where the complex physics of supersaturation and droplet condensation is treated in a simplified framework of passive scalars.

Fluctuations of passive scalar  $\theta$  at scales smaller than the Kolmogorov length  $\bar{\eta}$  are assumed to be convected by random straining motion, which is approximately uniform over the domain of size of  $\bar{\eta}$ . In local coordinates such that the rate of the strain tensor  $e_{ij} = (1/2)(\partial u_i/\partial x_j + \partial u_j/\partial x_i)$  is diagonal, the velocity field is expressed as  $\mathbf{u} = \alpha x_1 \mathbf{e}_1 + \beta x_2 \mathbf{e}_2 + \gamma x_3 \mathbf{e}_3$ , where the eigenvalues  $\alpha, \beta$

and  $\gamma$  are ordered as  $\gamma < \beta < \alpha$  and  $\mathbf{e}_i$ 's are the corresponding eigenvectors. The equation for  $\theta$  in the small blob is given as

$$\frac{\partial \theta}{\partial t} + \frac{\partial}{\partial x_1}(\alpha x_1 \theta) + \frac{\partial}{\partial x_2}(\beta x_2 \theta) + \frac{\partial}{\partial x_3}(\alpha x_3 \theta) = \kappa \nabla^2 \theta. \quad (1)$$

The scalar blob is quickly squeezed into a smaller size under the fluid motion of  $\gamma x_3$  ( $\gamma < 0$ ) until the molecular diffusion balances, and then the equilibrium state is established and characterized by

$$-|\gamma| \frac{d}{dx_3}(x_3 \theta) = \kappa \frac{d^2 \theta}{dx_3^2}. \quad (2)$$

The equation of the two-point correlation function of the scalar is given by

$$-|\gamma| r \frac{d\langle \theta \theta' \rangle}{dr} = 2\kappa \frac{d^2 \langle \theta \theta' \rangle}{dr^2}, \quad (3)$$

where  $\theta' = \theta(\mathbf{x} + r\mathbf{e}_3)$  and  $r$  is the separation distance along the direction of the least eigenvalue of the rate of the strain tensor [12]. The corresponding equation of the scalar spectrum  $E_\theta$  in the statistically isotropic state at small scales can be obtained as [12,15]

$$|\gamma| \frac{d}{dk} k E_\theta(k) = -2\kappa k^2 E_\theta(k). \quad (4)$$

Here Batchelor replaced  $|\gamma|$  by  $C_B^{-1}(\bar{\epsilon}/\nu)^{1/2}$  because  $\gamma$  is fluctuating, where  $C_B > 0$  is the Batchelor constant and  $\bar{\epsilon}$  is the mean dissipation rate of the kinetic energy per unit mass. The scalar spectrum is then easily obtained as

$$E_\theta(k) = C_B \bar{\chi}_\theta \left(\frac{\bar{\epsilon}}{\nu}\right)^{-1/2} k^{-1} e^{-C_B(k\bar{\eta}_B)^2}, \quad (5)$$

where  $\bar{\chi}_\theta$  is the mean dissipation rate of the scalar variance and  $\bar{\eta}_B = \bar{\eta} \text{Sc}^{-1/2} \ll \bar{\eta}$  is the Batchelor length. When  $k\bar{\eta}_B \ll 1$ , the viscous-convective range exists and  $E_\theta(k)$  is

$$E_\theta(k) = C_B \bar{\chi}_\theta \left(\frac{\bar{\epsilon}}{\nu}\right)^{-1/2} k^{-1}. \quad (6)$$

It is important to note that when both the Reynolds number and Schmidt number are very high the inertial-convective range ( $k_L \ll k \ll k_d = 1/\bar{\eta}$ ) and the viscous-convective range ( $k_d \ll k \ll k_B = 1/\bar{\eta}_{Bs}$ ) exist, and the scalar flux injected at  $k_L$  is constant and equal to  $\bar{\Pi}_\theta = \bar{\chi}_\theta$  throughout the two ranges  $k_L \ll k \ll k_B$  according to Yaglom's 4/3 law [13,18–20].

The  $k^{-1}$  spectrum is theoretically valid at wave numbers much higher than  $k_d$ . However, some studies have shown that the  $k^{-1}$  spectrum is observed at much lower wave numbers [10,21–24]. For the moment, we put aside the theoretical condition  $k \gg k_d$  and see where  $k^{-5/3}$  and  $k^{-1}$  spectra match. In the inertial-convective range  $E_\theta(k)$  is

$$E_\theta(k) = C_{oc} \bar{\chi}_\theta \bar{\epsilon}^{-1/3} k^{-5/3}, \quad (7)$$

where  $C_{oc}$  is the Obukhov-Corrsin constant [25–27]. Given the requirement that the spectrum of Eq. (7) matches the spectrum of Eq. (6) at  $k_*$ , the transition wave number yields

$$k_* \bar{\eta} = \left(\frac{C_{oc}}{C_B}\right)^{3/2} \approx 0.038. \quad (8)$$

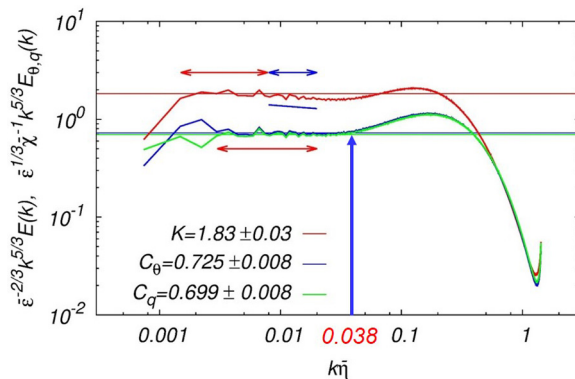


FIG. 1. Compensated spectra of kinetic energy and scalar variances. Red:  $\bar{\epsilon}^{-2/3} k^{5/3} E(k)$ ; blue:  $\bar{\chi}_\theta^{-1} \bar{\epsilon}^{1/3} k^{5/3} E_\theta(k)$  (excited by Gaussian random injection); green:  $\bar{\chi}_q^{-1} \bar{\epsilon}^{1/3} k^{5/3} E_q(k)$  (excited by the mean uniform gradient) [14]. Collapse of two curves of the scalar spectra except the low wave-number range indicates the fact that the scaling of the scalar spectrum is not affected by the scalar gradient.

The Obukhov-Corrsin and Batchelor constants are 0.7 and 6.2, respectively, through DNS, as described in the following. The computed transition wave number  $k_*\bar{\eta} = 0.038 = (0.7/6.2)^{3/2}$  is much smaller than the condition  $k\bar{\eta} \gg 1$  that the Batchelor theory assumes; rather, it is approximately at the upper end of the inertial convective range. Indeed, as seen in Fig. 1, the bump features in the compensated spectra  $\bar{\chi}_\theta^{-1} \bar{\epsilon}^{1/3} k^{5/3} E_\theta(k)$  and  $\bar{\chi}_q^{-1} \bar{\epsilon}^{1/3} k^{5/3} E_q(k)$  for the variances of passive scalars  $\theta$  and  $q$ , respectively, and  $\bar{\epsilon}^{-2/3} k^{5/3} E(k)$  for the kinetic energy obtained by DNS begin at wave numbers very close to  $k_*\bar{\eta} = 0.038$ , where  $\theta$  and  $q$  are convected by the same isotropic turbulence and excited by different scalar injection methods that are described below [14].

For  $C_{oc}$ , we use a DNS with the number of grid points at  $4096^3$ ,  $R_\lambda = 803$ , and  $Sc = 0.72$  [14]. The velocity is maintained by a random force corresponding to Gaussian white noise.  $\theta$  is excited by the Gaussian random noise of the Ornstein-Uhlenbeck process, and  $q$  by the mean uniform scalar gradient.

The two compensated spectra collapse well and are horizontal for  $0.002 < k\bar{\eta} < 0.03$ , meaning that  $E_\theta(k)$  and  $E_q(k)$  follow the  $k^{-5/3}$  spectrum, from which the Obukhov-Corrsin constants are evaluated as  $C_\theta = 0.725$  and  $C_q = 0.699$ , respectively, and we take  $C_{oc} \approx 0.7$ . The horizontal curves begin to increase at about  $k_*\bar{\eta} = 0.038$ , with a slope close to  $1/3$  that is slightly smaller than  $2/3 = -1 + 5/3$ , which is known as the spectral bump. There is an explanation for the bump formation, such that one of the legs in the triad interaction is lost, due to the molecular dissipation [28]. However, it is not certain at this point whether the same physics can be applied to Eq. (8).

The excellent agreement of  $k_*\bar{\eta} = 0.038$  with DNS data suggests that turbulent straining motion is acting on the passive scalar as if the rate of the strain tensor is effectively uniform over the domain of size  $1 \ll r/\bar{\eta} < 1/0.038$  if the same mechanisms as the one by Batchelor can be applied to this domain. Given that the viscosity is irrelevant in this range, we consider that it is not appropriate to call this wave-number range the viscous-convective range. Alternatively, we refer to this range as the *strain-convective (SC) range* in this study. It should be noted that the transition wave number (frequency) of the LWC spectrum found in field measurements is one order smaller than  $k_*\bar{\eta} = 0.038$ .

Given that the above DNS for the passive scalar was made at  $Sc = 0.72$ , the molecular diffusivity may introduce some ambiguity in interpretation of the above results. To make the physical setup simpler and more transparent, an alternative numerical simulation method for computing the scalar spectrum at an infinite Schmidt number was applied; the details are reported elsewhere [29]. Here we provide a brief description of the method and the results that are especially relevant for the present study.

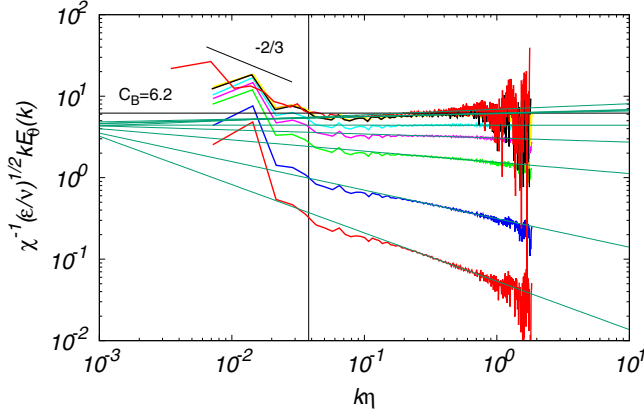


FIG. 2. Compensated three-dimensional spectra of scalar variance carried by particles  $\bar{\chi}^{-1}(\bar{\epsilon}/\nu)^{1/2}kE_{\theta}(k)$ . The curves are plotted from top to bottom for increasing  $D_k = \tau_k/\tau_{\theta}$ , where  $\tau_{\theta}$  is the scalar relaxation time of the particle. The top curve is for  $R_{\lambda} = 387$  and the others for 225, respectively. The Batchelor constant  $C_B = 6.2$  is computed for  $\tau_p = 200$ . Vertical thin line indicates  $k\bar{\eta} = 0.038$ .

Scalar transport via temperature, as an example, by monodisperse particles that are convected by turbulence is assumed to obey the equations

$$\frac{d\mathbf{X}_j(t)}{dt} = \mathbf{u}(\mathbf{X}_j(t), t), \quad (9)$$

$$\frac{D\theta_p}{Dt} = -\frac{\theta_p(\mathbf{x}, t)}{\tau_{\theta}} + F_{\theta}(\mathbf{X}_j(t), t), \quad (10)$$

where  $\frac{D}{Dt} = \partial/\partial t + \mathbf{u} \cdot \nabla$ ,  $\mathbf{X}_j(t)$  is the position of the  $j$ th particle, and  $\theta_p(\mathbf{X}_j(t), t)$  is the particle temperature given by

$$\theta_p(\mathbf{x}, t) = \frac{c_p}{\rho_0 c_0} \sum_{j=1}^{N_p} m_j \theta_j \delta[\mathbf{x} - \mathbf{X}_j(t)], \quad (11)$$

and  $\tau_{\theta}$  is the relaxation time of the particle temperature. Here  $\theta_j$  and  $m_j$  represent the particle temperature and mass, respectively, and  $c_0$  and  $\rho_0$  are the specific heat and density of the fluid, respectively.  $c_p$  is the specific heat of the particle, and  $N_p$  is the number of particles inside a grid cell.  $F_{\theta}$  is the Gaussian random noise, whose spectral support is at low wave numbers. The computation of Eqs. (9) and (10) is made with the Lagrangian method. The fluid velocity at the particle position is linearly interpolated and the particle temperature as a continuum is computed at the grid points of the fluid by the linear interpolation. The spectrum of the fluctuation variance of the particle temperature is computed using fast Fourier transform analysis, by subtracting the shot noise due to the discreteness of the particle and by removing the spatial filter effects arising from the linear interpolation [30]. Thus, the obtained spectrum of the particle temperature (as a passive scalar) corresponds to that for an infinite Schmidt number.

The DNSs were done with  $N = 512^3$  grid points,  $k_{\max}\bar{\eta} = 1.61$  at  $R_{\lambda} = 225$  for most of runs and  $N = 1024^3$ ,  $k_{\max}\bar{\eta} = 1.58$  for  $R_{\lambda} = 378$ . Figure 2 shows the variation in the compensated spectrum  $\bar{\chi}^{-1}(\bar{\epsilon}/\nu)^{1/2}kE_{\theta}(k)$  for Damköhler number  $D_k$ , defined as

$$D_k = \frac{\tau_k}{\tau_{\theta}} = ((\bar{\epsilon}/\nu)^{1/2}\tau_{\theta})^{-1}, \quad (12)$$

where  $\tau_k = (\bar{\epsilon}/\nu)^{-1/2}$  is the Kolmogorov time. At low wave numbers the spectrum is close to  $k^{-5/3}$  and becomes horizontal at around  $k\bar{\eta} \approx 0.038$  when  $D_k$  is very small (large  $\tau_{\theta}$ ), meaning that the

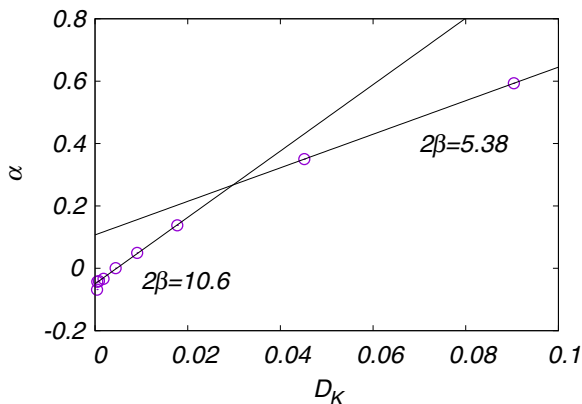


FIG. 3. Variation of exponent  $\alpha$  in Eq. (14) against  $D_\kappa$ . Straight lines show the slope  $2\beta = 10.6$  and  $5.38$ , respectively.

transition from  $k^{-5/3}$  to  $k^{-1}$  occurs at  $k\bar{\eta} = 0.038$ . When  $D_\kappa$  increases, the slope of the compensated spectrum decreases, as expected from the decay term in Eq. (10); however, the transition point remains unchanged.

Let us apply the Batchelor theory to the above particle temperature spectrum. The point is that the velocity field is assumed to be smooth and treated as linear in the local coordinates. The spectrum equation in the steady state is then given by

$$\frac{1}{\beta} \left( \frac{\bar{\epsilon}}{\nu} \right)^{-1/2} \frac{d}{dk} k E_\theta(k) = -\frac{2}{\tau_\theta} E_\theta(k), \quad (13)$$

where  $|\gamma|$  in Eq. (4) is replaced by the representative Kolmogorov timescale  $\beta^{-1}(\bar{\epsilon}/\nu)^{-1/2}$ , and  $\beta(> 0)$  is a positive constant. The solution is given by

$$k E_\theta(k) \propto \bar{\chi}_\theta \left( \frac{\bar{\epsilon}}{\nu} \right)^{-1/2} (k\bar{\eta})^{-2\beta D_\kappa} \propto k^{-\alpha}. \quad (14)$$

The spectrum obeys the power law, and the slope of  $k E_\theta(k)$  decreases with an increase in  $D_\kappa$ , which is consistent with the observation in Fig. 2. The computed exponent  $\alpha$  against  $D_\kappa$  is shown in Fig. 3. For small  $D_\kappa$ , the slope of the curve is  $2\beta = 10.6$ , such that  $\beta = 5.3$  is close to  $C_B = 6.2$ . In the analysis to follow, we use  $\beta = C_B$ .

We now return to the Batchelor's problem. The spectral equation of the passive scalar in the steady state can be written as

$$-\frac{d}{dk} \Pi_\theta(k) = T_\theta(k) = 2\kappa k^2 E_\theta(k), \quad (15)$$

where  $\bar{\Pi}_\theta$  is the transfer flux of the scalar variance across the wave number  $k$  from the band below  $k$  to the one above it. The above DNS data and arguments seem to strongly suggest that in the upper end of the inertial-convective range for the passive scalar spectrum, the transfer function can well be approximated as

$$-\frac{d}{dk} \Pi_\theta(k) = T_\theta(k) \approx -\frac{1}{C_B} \left( \frac{\bar{\epsilon}}{\nu} \right)^{1/2} \frac{d}{dk} k E_\theta(k). \quad (16)$$

Although the precise mechanism of the successful approximation is not known, and given the excellent agreement of the analytical results with DNS data, we will use this approximation in the latter analysis.

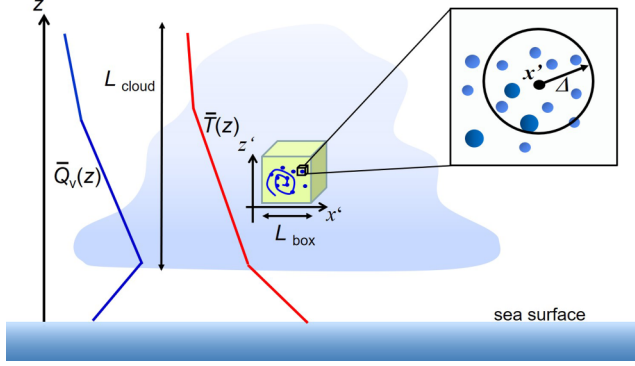


FIG. 4. Domain of cloud turbulence under the consideration. There is a small cubic box of size  $L_{\text{box}}$  well inside a cumulus cloud with characteristics length  $L_{\text{cloud}} \gg L_{\text{box}}$ . Mean water vapor mixing ratio  $\bar{Q}_v(z)$  and mean temperature  $\bar{T}(z)$  vary along the vertical direction, and the mean gradients  $\Gamma_T = d\bar{T}/dz$  and  $\Gamma_q = d\bar{Q}_v/dz$  are assumed to be constant over the cubic domain. The local coordinate system  $\mathbf{x}'$  is introduced. Inside the cubic domain, small sphere with radius  $\Delta$  centered on  $\mathbf{x}'$  is taken for coarse graining of the distribution of the water droplets.

### III. GOVERNING EQUATIONS

In this section, we show how, starting from a microscopic description of a cloud, a discrete distribution of particles can be treated as a continuum by coarse graining, and how the essential physical mechanisms governing the spectral dynamics of water vapor and liquid water fluctuations can be derived. The different assumptions are presented, allowing to arrive at a set of two coupled scalar equations (40) and (41). These will be the principal result of this section.

We consider a small domain well inside the cloud whose typical size  $L_{\text{box}}$  (say tens of meters) is much smaller than the whole cloud size  $L_{\text{cloud}}$  (about a few kilometers) (see Fig. 4). Also, there exist uniform mean gradients of the water vapor and temperature,  $\Gamma_T = d\bar{T}/dz$  and  $\Gamma_q = d\bar{Q}_v/dz$ , respectively, along the vertical direction. The water vapor mixing ratio  $q_v$ , the liquid water mixing ratio  $q_l$ , and the condensation-evaporation rate are defined as

$$q_v(\mathbf{x}, t) = \frac{m_v}{m_a}, \quad (17)$$

$$q_l(\mathbf{x}, t) = \frac{m_l}{m_a} = \frac{4\pi\rho_l}{3\rho_a\Delta^3} \sum_{j=1}^{N_\Delta(\mathbf{x}, t)} R_j^3(t), \quad (18)$$

$$\begin{aligned} C_d(\mathbf{x}, t) &\equiv \frac{1}{m_{\text{air}}} \frac{dm_l(\mathbf{x}, t)}{dt} \\ &= \frac{4\pi\rho_l K}{\rho_a\Delta^3} \sum_{k=1}^{N_\Delta(\mathbf{x}, t)} R_j(t) s(\mathbf{X}_j(t), t), \end{aligned} \quad (19)$$

respectively, where

$$R_j(t) \frac{dR_j(t)}{dt} = K_s s(\mathbf{X}_j(t), t) \quad (20)$$

is used [30–32]. Here  $m_v$ ,  $m_a$ , and  $m_l$  are the masses of the water vapor, dry air, and liquid water in a small cell of  $\Delta^3$ , respectively.  $\rho_l$  and  $\rho_a$  are the densities of water and the dry air, respectively,  $K_s$  is the temperature-dependent diffusion coefficient,  $N_\Delta(\mathbf{x}, t)$  is the number of droplets in the sphere with radius  $\Delta$  at position  $\mathbf{x}$  and time  $t$ , and  $\mathbf{X}_j$  and  $R_j$  are the position and radius of the  $j$ th droplet,

respectively.  $s$  is the supersaturation, which is defined by

$$s = \frac{q_v}{q_{vs}} - 1. \quad (21)$$

Here  $q_{vs}$  is the saturation water vapor mixing ratio at a given temperature and pressure.

Because the liquid water mixing ratio corresponds to the LWC spectrum, we refer to the above variance spectrum as the LWC spectrum in this study. Unlike air and water vapor, which are gases as a continuum form, the description of  $q_l$  differs from the gas phase as the typical number density of water droplets in cloud is on the order of hundreds to thousands per cubic centimeter.

For the continuum description of  $q_l$  it is necessary to introduce coarse graining in space with a certain size  $\Delta$  which is defined by

$$A_\Delta(\mathbf{x}, t) = \mathcal{P}[A] \equiv \frac{1}{N_\Delta(\mathbf{x}, t)} \sum_{j=1}^{N_\Delta(\mathbf{x}, t)} A[\mathbf{X}_j(t)], \quad (22)$$

where  $A$  is any quantity attributed to a droplet at  $\mathbf{X}_j(t)$ .  $\Delta$  needs to be as large as  $\Delta^3$  to contain a sufficient number of droplets. Thus, we assume that  $\Delta$  is at least larger than about half a centimeter, fivefold longer than the typical Kolmogorov length  $\bar{\eta}$  of 1 mm, but much shorter than the Taylor microscale that is about 50-fold the Kolmogorov length. The liquid water content mixing ratio  $q_l(\mathbf{x}, t)$  as a continuum is then given by

$$\begin{aligned} q_{l\Delta}(\mathbf{x}, t) &= \mathcal{P}[q_l] \\ &= \frac{4\pi}{3} \frac{\rho_l}{\rho_a} \frac{N_\Delta(\mathbf{x}, t)}{\Delta^3} \frac{1}{N_\Delta(\mathbf{x}, t)} \sum_{j=1}^{N_\Delta(\mathbf{x}, t)} R_j^3(t) \\ &\approx \lambda n_\Delta(\mathbf{x}, t) \bar{R}^3(t), \quad \lambda = \frac{4\pi}{3} \frac{\rho_l}{\rho_a}, \end{aligned} \quad (23)$$

where  $n_\Delta(\mathbf{x}, t)$  is the number density of the droplets; here, the passage from the second line to the third line replaces the local average of the cubic radius  $R^3$  by  $\bar{R}^3$  the cube of its mean  $\bar{R}$ . Similarly, the continuum representation of the condensation-evaporation rate  $C_d$  is as follows:

$$\begin{aligned} C_{d\Delta}(\mathbf{x}, t) &= \mathcal{P}[C_d] \\ &= \frac{4\pi}{3} \frac{\rho_l}{\rho_a} \frac{N_\Delta(\mathbf{x}, t)}{\Delta^3} \frac{1}{N_\Delta(\mathbf{x}, t)} \sum_{j=1}^{N_\Delta(\mathbf{x}, t)} \frac{dR_j^3(t)}{dt} \\ &= \frac{4\pi}{3} \frac{\rho_l}{\rho_a} \frac{N_\Delta(\mathbf{x}, t)}{\Delta^3} \bar{R}^3 \frac{3K}{\bar{R}^2} \frac{1}{N_\Delta(\mathbf{x}, t)} \sum_{j=1}^{N_\Delta(\mathbf{x}, t)} \left( \frac{R_j}{\bar{R}} \right) s(\mathbf{X}_j(t), t) \\ &\approx \frac{1}{\tau_l} q_{l\Delta}(\mathbf{x}, t) s_\Delta(\mathbf{x}, t), \end{aligned} \quad (24)$$

where  $s_\Delta$  is the coarse-grained supersaturation, and Eq. (20) and the approximation  $(R_j / \bar{R}) \approx 1$  are used. The timescale  $\tau_l$ , defined by

$$\tau_l = \frac{\bar{R}^2}{3K}, \quad (25)$$

characterizes the condensation-evaporation process and is in proportion to the square of the mean droplet radius in the domain [33]. It should be stressed also that  $\tau_l$  is independent of the scale (wave number).



The next step is to derive the equation for  $q_{l\Delta}(\mathbf{x}, t)$  as continuum. Let us consider the change in the liquid water mass in  $\Delta^3$ . Physical processes contributing to the change in mass are (1) transfer by flow, (2) molecular diffusion, (3) nucleation, (4) condensation-evaporation, (5) collision and coalescence, (6) break-up, and (7) the fallout of droplets. Process (1) is expressed as the Eulerian convective term  $\mathbf{u} \cdot \nabla q_{l\Delta}$ . Number (2) is neglected, as the typical size of droplets is about ten micron meters, and the Brownian motion of droplets estimated with Einstein's formula is negligible. For (3), we assume that the mean supersaturation of the water vapor is zero for simplicity [more arguments follow after Eq. (35)]; thus, this contribution is eliminated. Point (4) is a key process in the present study to be included. For (5) and (6), the typical radius of droplets under consideration is about ten micron meters, such that the contributions of the collision-coalescence and break-up processes are very small and, thus, are not included. Regarding (7), the removal of droplets due to sedimentation may be expressed as  $-q_l/\tau_r$ , where  $\tau_r$  is the characteristic time of droplet removal that is constant and considerably longer than the large eddy turnover time of  $L_{\text{box}}/u'$ , where  $u'$  is the root mean square velocity of the turbulence within the box [34,35].

We assume that the buoyancy force due to the condensation-evaporation is weak and can be neglected because  $L_{\text{box}} \ll L_{\text{cloud}}$ . The two scalars  $q_{v\Delta}$  and  $q_{l\Delta}$  interact with each other but not with the fluid motion; thus, they are treated as passive scalars for simplicity. Under these conditions, the fundamental equations are the Navier-Stokes equation for an incompressible fluid and the advection diffusion equations for  $q_{v\Delta}$  and  $q_{l\Delta}$  as

$$\left( \frac{\partial}{\partial t} + \mathbf{u} \cdot \nabla \right) \mathbf{u} = -\nabla p + \nu \nabla^2 \mathbf{u} + \mathbf{f}^u, \quad (26)$$

$$\nabla \cdot \mathbf{u} = 0, \quad (27)$$

$$\frac{\partial q_{v\Delta}}{\partial t} + \mathbf{u} \cdot \nabla q_{v\Delta} = \kappa_v \nabla^2 q_{v\Delta} - \frac{1}{\tau_l} q_{l\Delta} s_\Delta + \Gamma_q u_3, \quad (28)$$

$$\frac{\partial q_{l\Delta}}{\partial t} + \mathbf{u} \cdot \nabla q_{l\Delta} = \frac{1}{\tau_l} q_{l\Delta} s_\Delta - \frac{1}{\tau_r} q_{l\Delta}, \quad (29)$$

respectively.

For convenience, the water vapor mixing ratio  $q_{v\Delta}$  is changed to the supersaturation  $s_\Delta$  for further analysis. For this purpose we follow the steps used in [36], by using Eq. (21) and the Clausius-Clapeyron equation for relating the saturation pressure to the temperature. After dropping the subscript  $\Delta$  to be more concise, we obtain the equations for supersaturation and the liquid water mixing ratio as

$$\frac{\partial s}{\partial t} + \mathbf{u} \cdot \nabla s = \kappa_s \nabla^2 s - \frac{J}{\tau_l} q_l s + \Gamma_s u_3, \quad (30)$$

$$\frac{\partial q_l}{\partial t} + \mathbf{u} \cdot \nabla q_l = \frac{1}{\tau_l} q_l s - \frac{1}{\tau_r} q_l, \quad (31)$$

where  $\Gamma_s = \Gamma_q/q_{vs}$  and  $\kappa_s$  is the diffusion constant for supersaturation. Also the equation for the absolute temperature  $T$  is given by

$$\frac{\partial T}{\partial t} + \mathbf{u} \cdot \nabla T = \kappa_T \nabla^2 T + \frac{L_v}{c_p \tau_l} q_l s - \frac{g}{c_p} u_3, \quad (32)$$

where  $\kappa_T$  is the temperature diffusion constant,  $c_p$  the specific heat for constant pressure,  $L_v$  the latent heat, and  $g$  is the gravitational acceleration. A nondimensional constant  $J$  arises from the variation of  $q_{vs}$  through the temperature [36] and

$$J = \frac{P}{\epsilon e_s} + \frac{\epsilon L_v^2}{c_p R_d T^2}, \quad (33)$$

where  $P$  is the static pressure,  $\epsilon = R_d/R_v = 0.62$ ,  $e_s$  the saturation pressure, and  $R_d$  and  $R_v$  are the gas constants for dry air and water vapor, respectively.

We now define for latter use the relaxation time of the supersaturation  $\tau_s$  as

$$\frac{1}{\tau_s} = J \frac{\bar{Q}_l}{\tau_l} = J(4\pi K \bar{n}_d \bar{R}) \left( \frac{\rho_l}{\rho_a} \right). \quad (34)$$

Here  $\bar{n}_d$  and  $\bar{Q}_l$  are the means of the number density and the water vapor mixing ratio, respectively.

Let us write the variables as the sum of the mean and fluctuation, as

$$s = \bar{S} + \tilde{s}, \quad q_l = \bar{Q}_l + \tilde{q}_l, \quad T = \bar{T} + \tilde{\theta}, \quad (35)$$

where  $\bar{S} = \langle s \rangle$ ,  $\bar{Q}_l = \langle q_l \rangle$ ,  $\bar{T} = \langle T \rangle$ , and  $\langle \rangle$  denotes the ensemble average. We assume that the turbulent field is statistically steady and homogeneous and the fluctuations are much smaller than the means. Substitution of Eq. (35) into Eqs. (30), (31), and (32) leads to the equations for the means as

$$\frac{d\bar{S}(t)}{dt} = -\frac{J}{\tau_l} (\bar{Q}_l \bar{S} + \langle \tilde{q}_l \tilde{s} \rangle), \quad (36)$$

$$\frac{d\bar{Q}_l(t)}{dt} = \frac{1}{\tau_l} (\bar{Q}_l \bar{S} + \langle \tilde{q}_l \tilde{s} \rangle) - \frac{\bar{Q}_l}{\tau_r}, \quad (37)$$

$$\frac{d\bar{T}(t)}{dt} = \frac{L_v}{c_p \tau_l} (\bar{Q}_l \bar{S} + \langle \tilde{q}_l \tilde{s} \rangle), \quad (38)$$

where  $\nabla \langle \mathbf{u} \tilde{s} \rangle = \nabla \langle \mathbf{u} \tilde{q}_l \rangle = \nabla \langle \mathbf{u} \tilde{\theta} \rangle = 0$  via the homogeneity is applied. When  $J$  is constant in time and  $\tau_r$  is very large so that the second term of the r.h.s. of Eq. (37) is neglected, it is easily found from Eqs. (36) and (37) that  $d(\bar{S} + J\bar{Q}_l)/dt = 0$  so that the weighted sum  $(\bar{S} + J\bar{Q}_l)$  is constant in time. If the fluctuating part  $\langle \tilde{q}_l \tilde{s} \rangle$  is neglected, Eq. (36) means that  $\bar{S}(t)$  vanishes at latter times because  $\bar{Q}_l(t) > 0$ , unless there is injection of the systematic (mean) supersaturation from outside. Therefore, in this study we assume that  $\bar{S}(t) = 0$  and the fluctuating term  $\langle \tilde{q}_l \tilde{s} \rangle / \bar{Q}_l$  can be neglected; thus, the right-hand side of Eq. (36) vanishes, consistent with  $\bar{S}(t) = 0$ . A similar argument can be applied to the right-hand side of (38), so that  $\bar{T}(t)$  is constant in time. When there exists the mean uniform gradient  $\Gamma_T$  along the vertical direction, this implies that  $\bar{T} = T_0 + \Gamma_T z$  is constant in time, where  $T_0$  is mean temperature in the box. On the other hand, Eq. (37) implies that  $\langle \tilde{q}_l \tilde{s} \rangle / \bar{Q}_l = \tau_l / \tau_r \ll 1$  is necessary for the steady state to be achieved. As such, we drop the term of  $1/\tau_r$  in the sense of  $\tau_l \ll \tau_r$  in the present analysis.

Given that  $q_l$  is positive definite, it is convenient to work with its logarithm as

$$\begin{aligned} q_l &= \bar{Q}_l + \tilde{q}_l > 0, \\ \log q_l &= \ln \bar{Q}_l + \ln(1 + \phi), \\ &\approx \ln \bar{Q}_l + \phi, \quad \phi = \frac{\tilde{q}_l}{\bar{Q}_l}, \end{aligned} \quad (39)$$

where the fluctuation  $\tilde{q}_l/\bar{Q}_l$  is assumed to be small in the last line. Substituting Eqs. (35) and (39) into Eqs. (30) and (31), subtracting Eqs. (36) and (37) from the resulting equations, and using the assumption  $\bar{S} = 0$  and neglecting the second-order terms in the fluctuations, we obtain the equations for the fluctuations of the supersaturation  $s$  [37,38] and the (normalized) LWC  $\phi$  as

$$\frac{\partial s}{\partial t} + \mathbf{u} \cdot \nabla s = -\frac{1}{\tau_s} s + \kappa_s \nabla^2 s + \Gamma_s u_3, \quad (40)$$

$$\frac{\partial \phi}{\partial t} + \mathbf{u} \cdot \nabla \phi = \kappa_\phi \nabla^2 \phi + \frac{1}{\tau_l} s, \quad (41)$$

where  $\tilde{\cdot}$  of  $\tilde{s}$  is again dropped for ease of writing. Also the temperature fluctuation obeys the equation

$$\frac{\partial \theta}{\partial t} + \mathbf{u} \cdot \nabla \theta = \kappa_\theta \nabla^2 \theta + \Gamma_\theta u_3 + \frac{L_v}{c_p \tau_s} s, \quad (42)$$

where  $\Gamma_\theta = \Gamma_T - g/c_p$ .

We observe the following: (1) The supersaturation  $s$  is damped at the constant rate  $1/\tau_s$  in addition to the molecular diffusivity and excited by the turbulent velocity through the mean uniform gradient  $\Gamma_s$ . On the other hand, (2) the LWC and temperature fluctuations are dissipated only by the diffusion term, but excited by the supersaturation  $s$  at the rates  $1/\tau_l$  for the LWC and  $L_v/(c_p \tau_l)$  for the temperature, respectively, and excited also by  $\Gamma_s u_3$  for the temperature.

These facts indicate that the temperature fluctuations affect indirectly  $s$  and  $\phi$  through the characteristic times  $\tau_s$ ,  $\tau_l$  and the mean gradient for the supersaturation  $\Gamma_s = \Gamma_q/q_{vs}$  via  $J$ ,  $K_s$ , and  $q_{vs}$ . Therefore, it is reasonable to primarily consider two equations for the supersaturation and the LWC, and we neglect the temperature fluctuation effects. Equations (40) for the supersaturation and (41) for the LWC are main results of this section.

Note that the diffusive term in Eq. (41) is now added, based on the following. The properties of  $q_{v\Delta}$  ( $s_\Delta$ ) and  $q_{l\Delta}$  ( $\phi_\Delta$ ) as continuum below the size  $\Delta$  are lost due to the coarse graining, in which the loss of information appears as memory decay effects, which is well known in nonequilibrium statistical mechanics [39]. A simple way to represent this is to introduce the effective diffusivity  $\kappa_\phi$ . The amplitude of the effective diffusivity is estimated as  $\kappa_\phi \sim u_\Delta \Delta$  on the dimensional ground where  $u_\Delta$  is the velocity at the scale of  $\Delta$ . An estimate of  $\kappa_\phi$  may be obtained from the data of Ref. [6]. From the turbulence data  $\bar{\epsilon} = 8.5 \times 10^{-2} \text{ m}^2 \text{ s}^{-3}$  and  $\nu = 1.33 \times 10^{-5} \text{ m}^2 \text{ s}^{-1}$ , we have  $u_\Delta \sim (\bar{\epsilon}\nu)^{1/4} \approx 3.2 \times 10^{-2} \text{ m s}^{-1}$  and  $\Delta = \bar{\eta} \sim 4.1 \times 10^{-4} \text{ m}$ , such that the effective diffusivity is about  $\kappa_\phi \approx 1.3 \times 10^{-5} \text{ m}^2 \text{ s}^{-1}$ ; this is the same order as the kinetic viscosity and the effective Schmidt number  $\text{Sc}_\phi = \nu/\kappa_\phi \approx 1$ . A similar estimate can be applied to  $s_\Delta$  in which  $\kappa_s$  is understood to be the augmented diffusivity for supersaturation. However, since the wave-number range under the present consideration is much smaller than the diffusive wave-number range originating from the above coarse graining, the details of the diffusive effects are irrelevant for the present purpose. On the other hand, the fluid variables  $\mathbf{u}$  and  $p$  are free from the coarse graining, because the scalars are assumed to be passive in the present study.

Both equations for  $s$  and  $\phi$  are passive scalar equations convected by the turbulence. Unlike the conventional passive scalar equations, the equation for  $s$  contains a linear damping term whose timescale is scale-independent. Although  $\tau_l$  is the timescale of condensation-evaporation, it is not the timescale of the dynamics of  $\phi$ , but it controls the excitation by  $s$ .

Based on this discussion, it is important to estimate the characteristic times  $\tau_l$  and  $\tau_s$ . According to the data of October 26, 2009, of Ref. [6], the mean diameter of droplets is about  $13 \mu\text{m}$ , the mean number density is about  $275 \text{ cm}^{-3}$ , and we have  $\bar{Q}_l \approx 2.63 \times 10^{-4}$ ,  $J \approx 265$  at  $273 \text{ K}$ , and  $\tau_l \approx 0.13 \text{ s}$ ,  $\tau_s \approx 1.84 \text{ s}$ . For turbulence, using the values of  $\bar{\epsilon}$  and  $\nu$ , the Kolmogorov time is estimated to be  $\tau_k = (\nu^3/\bar{\epsilon})^{1/4} \approx 1.25 \times 10^{-2} \text{ s}$ . The large-scale  $L$  is estimated by  $\bar{\epsilon} = 0.4u'^3/L$ , where  $0.4$  is the value reported in the literature [40] and  $L \approx 13 \text{ m}$ , while  $\tau_L = L/u' \approx 9.3 \text{ s}$ . From these values, we obtain the characteristic times normalized by the Kolmogorov time as

$$\frac{\tau_s}{\tau_k} \approx 1.5 \times 10^2, \quad \frac{\tau_l}{\tau_k} \approx 1.0 \times 10^1, \quad \frac{\tau_L}{\tau_k} \approx 7.4 \times 10^2, \quad (43)$$

and the characteristic Damköhler numbers are

$$D_k = \frac{\tau_k}{\tau_s} \approx 6.7 \times 10^{-3}, \quad D_L = \frac{\tau_L}{\tau_s} \approx 5.1, \quad (44)$$

respectively.

## IV. SPECTRAL EQUATIONS

In this section, the spectral equations for the supersaturation and LWC variances are derived by using the LRA theory. The importance of the different timescales is stressed and the wave-number-dependent Damköhler number is introduced.

We now assume that the Reynolds number is very high and that the fluctuations of turbulent flow, the water vapor mixing ratio, and the liquid water content are statistically homogeneous, and the turbulence is further assumed to be statistically isotropic. The spectral densities are defined by

$$U_u(\mathbf{k}, t) = \frac{1}{2} \langle u_i(\mathbf{k}, t) u_i(-\mathbf{k}, t) \rangle, \quad (45)$$

$$U_s(\mathbf{k}, t) = \langle s(\mathbf{k}, t) s(-\mathbf{k}, t) \rangle, \quad (46)$$

$$U_\phi(\mathbf{k}, t) = \langle \phi(\mathbf{k}, t) \phi(-\mathbf{k}, t) \rangle, \quad (47)$$

where  $\mathbf{k}$  is the wave vector. Since there exists the mean uniform gradient of the supersaturation along the vertical direction, the two scalars are statistically axially symmetric and can be expanded in terms of Legendre polynomials as follows:

$$Q_A(\mathbf{k}) = Q_A(k) + Q_A^{(2)} P_2(\cos \theta) + \dots, \quad (48)$$

where  $A$  stands for  $s$  or  $\phi$  and  $P_{2n}(\cos \theta)$  is the  $2n$ -order Legendre polynomial [13,19]. However, given that the isotropy of the scalars is restored at small scales, provided that the Schmidt number is not too small, the contributions from higher-order Legendre polynomials can be neglected [19,41]. Therefore, we consider only the zeroth order (isotropic part) in what follows. The spectra of the kinetic energy and the scalar variances per unit mass are defined by

$$E_u(t) = \frac{1}{2} \langle \mathbf{u}^2(\mathbf{x}, t) \rangle \equiv \frac{3}{2} u^2(t) = \int_0^\infty E_u(k, t) dk, \quad (49)$$

$$E_s(t) = \langle s^2(\mathbf{x}, t) \rangle \equiv s^2(t) = \int_0^\infty E_s(k, t) dk, \quad (50)$$

$$E_\phi(t) = \langle \phi^2(\mathbf{x}, t) \rangle \equiv \phi^2(t) = \int_0^\infty E_\phi(k, t) dk, \quad (51)$$

respectively, where

$$E_u(k, t) = 2\pi k^2 U_u(k, t), \quad (52)$$

$$E_s(k, t) = 4\pi k^2 U_s(k, t), \quad (53)$$

$$E_\phi(k, t) = 4\pi k^2 U_\phi(k, t). \quad (54)$$

The spectral equations for the isotropic parts can be written as

$$\left( \frac{\partial}{\partial t} + 2\nu k^2 \right) E_u(k, t) = T_u(k, t) + F_u(k, t), \quad (55)$$

$$\left( \frac{\partial}{\partial t} + \frac{2}{\tau_s} + 2\kappa_s k^2 \right) E_s(k, t) = T_s(k, t) + F_s(k, t), \quad (56)$$

$$\left( \frac{\partial}{\partial t} + 2\kappa_\phi k^2 \right) E_\phi(k, t) = T_\phi(k, t) + F_\phi(k, t), \quad (57)$$

where  $T_A$  ( $A = u, s,$  or  $\phi$ ) is the transfer function defined by

$$T_u(k, t) = 4\pi k^2 \mathcal{R} \langle N_u(\mathbf{k}, t) \cdot \mathbf{u}(-\mathbf{k}, t) \rangle, \quad (58)$$

$$T_s(k, t) = 8\pi k^2 \mathcal{R} \langle C_s(\mathbf{k}, t) s(-\mathbf{k}, t) \rangle, \quad (59)$$

$$T_\phi(k, t) = 8\pi k^2 \mathcal{R}\langle C_\phi(\mathbf{k}, t)\phi(-\mathbf{k}, t) \rangle, \quad (60)$$

where  $\mathcal{R}$  denotes the real part,  $N_u(\mathbf{k}, t)$  is the Fourier transform of the convective plus pressure term for the velocity, and  $C_s$  and  $C_\phi$  are those of the convective terms.  $F_u$  is the forcing, and  $F_s$  and  $F_\phi$  are the scalar injections:

$$F_u(k, t) = 4\pi k^2 \mathcal{R}\langle \mathbf{f}_u(\mathbf{k}, t) \cdot \mathbf{u}(-\mathbf{k}, t) \rangle, \quad (61)$$

$$F_s(k, t) = \Gamma_s 8\pi k^2 \mathcal{R}\langle u_3(\mathbf{k}, t)s(-\mathbf{k}, t) \rangle, \quad (62)$$

$$F_\phi(k, t) = \frac{1}{\tau_l} 8\pi k^2 \mathcal{R}\langle \phi(\mathbf{k}, t)s(-\mathbf{k}, t) \rangle. \quad (63)$$

Equations (55), (56), and (57) indicate that the external force  $F_u(k, t)$  applied at large scales, say, a large-scale mean shear, maintains the turbulence  $E_u(k, t)$ , which excites the supersaturation  $E_s(k, t)$  through the mean uniform gradient by  $F_s(k, t)$ . Thus, excited supersaturation fluctuations  $E_s(k)$  drive the LWC fluctuations  $E_\phi(k, t)$  by  $F_\phi(k, t)$ . From this observation of the chain of excitations, we assume in what follows that the turbulent velocity and scalars are in a statistically steady state.

The next step is to obtain a closed set of spectral equations for the above three spectra. For this purpose, we use the Lagrangian renormalized approximation (LRA), which is a spectral closure theory fully formulated in the Lagrangian framework [42,43]. The properties of the LRA are that the procedure is fully systematic, no *ad hoc* parameters are contained, and the spectra of the kinetic energy and scalar variance are consistent with the Kolmogorov spectrum with a Kolmogorov constant of 1.72 and the Obukhov-Corrsin spectrum in the inertial-convective range [42–44].

Although we do not discuss the LRA in detail here, we provide a brief description of the derivation of the external source terms  $F_s(K, t)$  and  $F_\phi(k, t)$  in the LRA in a symbolic way to avoid complication, as  $F_s(K, t)$  and  $F_\phi(k, t)$  are key quantities for obtaining the spectra  $E_s(k)$  and  $E_\phi(k)$ , respectively, and because it is essential and useful to understand how the timescales of turbulence and phase relaxation affect the spectral dynamics. For details regarding the derivation of the LRA equations, the reader can consult Refs. [42,43].

Let us consider first the evolution of  $s$  in Eq. (40) in the Lagrangian frame moving along with a fluid particle. The supersaturation in the wave-vector space  $s^L(\mathbf{k}, t)$  at time  $t$  is written symbolically,

$$s^L(\mathbf{k}, t) = \int_{-\infty}^t G_s^L(\mathbf{k}, t, \xi) \Gamma_s u_3^L(\mathbf{k}, \xi) d\xi, \quad (64)$$

where  $G_s^L(\mathbf{k}, t, s)$  is the Lagrangian response function and  $u_3^L(\mathbf{k}, s)$  is the Lagrangian velocity. Substituting this into Eq. (62) and splitting the triple correlation into the product of the mean response function and the Lagrangian two-time correlation of the velocity, we have

$$\begin{aligned} F_s(k, t) &= 8\pi k^2 \Gamma_s^2 \int_{-\infty}^t \langle G_s^L(\mathbf{k}, t, \xi) u_3^L(\mathbf{k}, \xi) u_3^L(-\mathbf{k}, t) \rangle d\xi \\ &\approx 8\pi k^2 \Gamma_s^2 \int_{-\infty}^t \langle G_s^L(\mathbf{k}, t, \xi) \rangle \langle u_3^L(\mathbf{k}, \xi) u_3^L(-\mathbf{k}, t) \rangle d\xi. \end{aligned} \quad (65)$$

Here  $\langle u_3^L(\mathbf{k}, \xi) u_3^L(-\mathbf{k}, t) \rangle$  is the Lagrangian two-time velocity correlation, and we assume that

$$\langle u_3^L(\mathbf{k}, \xi) u_3^L(-\mathbf{k}, t) \rangle = e^{-(t-\xi)/\sigma(k)} P_{33}(k) U_u(k), \quad (66)$$

$$\langle G_s^L(\mathbf{k}, t, \xi) \rangle = e^{-(t-\xi)/\sigma_s(k)}, \quad (67)$$

where  $P_{ij}(\mathbf{k}) = \delta_{ij} - k_i k_j / k^2$  is the projection operator, and the characteristic times  $\sigma(k)$  and  $\sigma_s(k)$  are approximately given by

$$\frac{1}{\sigma(k)} = \nu k^2 + \left( \int_0^k p'^2 E_u(p') dp' \right)^{1/2}, \quad (68)$$

$$\frac{1}{\sigma_s(k)} = \frac{1}{\tau_s} + \kappa_s k^2. \quad (69)$$

In the inertial range, the energy spectrum is

$$E_u(k) = K \bar{\epsilon}^{2/3} k^{-5/3}, \quad (70)$$

where  $K$  is the Kolmogorov constant [27], and substitution yields the eddy turn over time at  $k$  as

$$\sigma(k) = \lambda_u \bar{\epsilon}^{-1/3} k^{-2/3}. \quad (71)$$

In what follows, we set  $\lambda_u = 1$  for making the analysis simpler, and when the wave-number-dependent timescale is intended, the argument  $k$  is explicitly written. Note that even for zero viscosity, the two-time velocity correlation (66) decays in time with the eddy damping rate  $\sigma(k)$  due to the pressure gradient. On the other hand, when  $\kappa_s$  is zero,  $\sigma_s(k)$  is equal to  $\tau_s$  which is independent of the wave number, so that  $\langle G_s^L \rangle$  decays at the phase relaxation time rate  $\tau_s$ . Fundamental idea of the eddy damping in the Lagrangian spectral theory is described in [42,45,46], and in [43,44] for the isotropic passive scalar and in [47] for the anisotropic passive scalar under mean scalar gradient.

Similarly, the expression for the LWC source term is given as

$$\begin{aligned} F_\phi(k, t) &= \frac{1}{\tau_l^2} 8\pi k^2 \langle \phi(\mathbf{k}, t) s(-\mathbf{k}, t) \rangle \\ &\approx \frac{1}{\tau_l^2} 8\pi k^2 \int_{-\infty}^t \langle G_\phi^L(\mathbf{k}, t, \xi) \rangle \langle s^L(\mathbf{k}, \xi) s^L(-\mathbf{k}, t) \rangle d\xi, \end{aligned} \quad (72)$$

where  $\langle s^L(\mathbf{k}, \xi) s^L(-\mathbf{k}, t) \rangle$  is the Lagrangian two-time correlation of the supersaturation. We assume that

$$\begin{aligned} \langle s^L(\mathbf{k}, \xi) s^L(-\mathbf{k}, t) \rangle_L &= G_s^L(\mathbf{k}, t, s) U_s(k) \\ &= e^{-(t-\xi)/\sigma_s(k)} U_s(k), \end{aligned} \quad (73)$$

$$\langle G_\phi^L(\mathbf{k}, t, \xi) \rangle = e^{-\kappa_\phi k^2 (t-\xi)}. \quad (74)$$

It should be noted that when  $\kappa_\phi = 0$ , the response function  $\langle G_\phi^L(\mathbf{k}, t, \xi) \rangle = 1$  does not decay at all, which is readily seen from Eq. (41). It is this difference in the characteristic times  $\sigma(k)$ ,  $\sigma_s(k)$ , and  $\sigma_\phi(k)$  that leads to the different behaviors of the transfer functions in spectral space.

Substitution of Eqs. (66) and (67) into Eq. (65) and of Eqs. (73) and (74) into Eq. (72) yields

$$F_s(k, t) = \frac{4}{3} \Gamma_s^2 \Theta_F(k) E_u(k), \quad (75)$$

$$F_\phi(k) = 2 \frac{\tau_s}{\tau_l^2} E_s(k), \quad (76)$$

and

$$\Theta_F(k) = \frac{\sigma(k)}{1 + \text{Da}(k)} \quad \text{for } k\bar{\eta} \ll 1, \quad (77)$$

$$\text{Da}(k) = \frac{\sigma(k)}{\tau_s}, \quad (78)$$

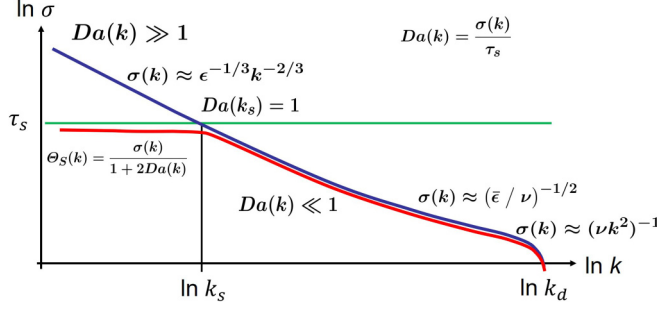


FIG. 5. Timescales of the triple relaxation  $\Theta_s(k)$  (red), the eddy turnover time  $\sigma(k)$  (navy), phase relaxation  $\tau_s$  (green), the straining time  $(\bar{\epsilon}/\nu)^{-1/2}$ , and the viscous dissipation time  $(\nu k^2)^{-1}$ .

where  $\Theta_F(k)$  is the characteristic time of the supersaturation source term and  $\text{Da}(k)$  is the wave-number-dependent Damköhler number.

The spectral equations for  $E_s(k)$  and  $E_\phi(k)$  in the steady state by the LRA are as follows:

$$2\left(\kappa_s k^2 + \frac{1}{\tau_s}\right)E_s(k) = T_s(k) + \frac{4}{3}\Gamma_s^2\Theta_F(k)E_u(k), \quad (79)$$

$$2\kappa_\phi k^2 E_\phi(k) = T_\phi(k) + 2\frac{\tau_s}{\tau_l^2} E_s(k), \quad (80)$$

and the transfer functions are

$$T_s(k) = 16\pi^2 k^3 \iint_{\Delta_k} dp dq pq(1-y^2)\Theta_s(k, p, q)U(q) [U_s(p) - U_s(k)], \quad (81)$$

$$T_\phi(k) = 16\pi^2 k^3 \iint_{\Delta_k} dp dq pq(1-y^2)\Theta_\phi(k, p, q)U(q) [U_\phi(p) - U_\phi(k)], \quad (82)$$

where  $\Delta_k$  denotes the domain of integrals satisfying  $\mathbf{k} = \mathbf{p} + \mathbf{q}$  and  $y$  is the cosine of the angle opposite to the leg  $p$  of the triangle with legs  $(k, p, q)$ .  $\Theta_s(k, p, q)$  and  $\Theta_\phi(k, p, q)$  are the triple relaxation time defined by

$$\Theta_s(k, p, q) = \frac{\sigma(q)}{1 + 2\text{Da}(q)}, \quad (83)$$

$$\Theta_\phi(k, p, q) = \sigma(q). \quad (84)$$

It should be noted that in the inertial-convective range, the  $\kappa_s k^2$  and  $\kappa_\phi k^2$  terms in  $\Theta_s$  and  $\Theta_\phi$  are neglected, and that only  $\sigma(q)$  controls  $T_\phi(k)$  and no  $\tau_s$  is included. The wave-number dependence of  $\Theta_s(k)$  and  $\sigma(k)$  are described in Fig. 5. The wave number  $k_s$  is defined at which the Damköhler number becomes unity as

$$\text{Da}(k_s) = 1, \quad \bar{\epsilon}^{-1/3} k_s^{-2/3} = \tau_s. \quad (85)$$

For  $k < k_s$ ,  $\Theta_s(k)$  tends to be more affected by  $\tau_s$  with a decrease in  $k$ ; whereas for  $k > k_s$ ,  $\sigma(k)$  controls the transfer of the supersaturation excitation in the inertial-convective range. In the upper end of the inertial range,  $\sigma(k)$  is considered to be nearly constant or very slowly decreasing in wave number until the diffusive time becomes important, as suggested in the DNS data (Sec. III). We note that the ratio  $\tau_s/\tau_\kappa \approx 1.5 \times 10^2$  in Eq. (43) implies  $k_s \bar{\eta} \sim (\tau_s/\tau_\kappa)^{-3/2} \approx 5.4 \times 10^{-4}$  which is well inside the inertial-convective range.

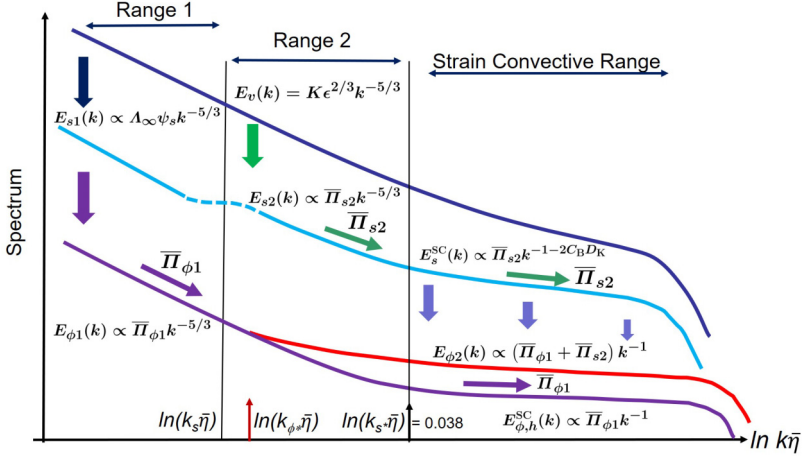


FIG. 6. Various ranges and spectra.  $\Lambda_\infty \psi_s$  and  $\Lambda_\infty (1 - \psi_s)$  are inputs for  $E_s(k)$  in the ranges 1 and 2 due to the turbulent velocity, respectively. In Range 1,  $E_{s1}$  excites  $E_{\phi_1}$  and  $\bar{\Pi}_{\phi_1}$  is transferred to the strain convective range without loss. In Range 2, the flux  $\bar{\Pi}_{s2}$  is transferred to the strain convective range without loss. In the strain convective range,  $E_s^{SC}(k)$  drives  $E_{\phi_2}^{SC}$  with an amplitude proportional to  $\bar{\Pi}_{s2}$ . The enhanced spectrum  $E_{\phi_2}^{SC}$  matches that of  $E_{\phi_1}$  at the transition wave number  $k_{\phi^*} \bar{\eta}$ .

## V. SCALING OF SUPERSATURATION SPECTRUM

In this section we consider the scaling of the supersaturation spectrum at very large Reynolds numbers. Because the turbulence is in a steady state, the kinetic energy spectrum in the inertial range is assumed to be the Kolmogorov spectrum (70). The analysis is made first for  $E_s(k)$  and then for  $E_\phi(k)$ . Figure 6 is a map of our analyses.

### A. Inertial-convective range

Because the spectrum of the input term of Eq. (79) has excitations at all wave numbers, it is important to know which wave-number range contributes most to the flux of the supersaturation variance. Integrating Eq. (79) from  $k_L$  to  $k$  ( $< k_s$ ), where  $k_L$  is the wave number of the supersaturation energy range or  $1/L_{\text{box}}$ , yields

$$\begin{aligned} \Pi_s(k) - \Pi_s(k_L) &= \int_{k_L}^k \frac{\partial \Pi(k')}{\partial k'} dk' = - \int_{k_L}^k T_s(k') dk' \\ &= -2\kappa_s \int_{k_L}^k k'^2 E_s(k') dk' - \frac{2}{\tau_s} \int_{k_L}^k E_s(k') dk' + \int_{k_L}^k F_s(k') dk'. \end{aligned} \quad (86)$$

In the literature, the mean scalar dissipation rate  $\bar{\chi}_s$  is used in the expression of the Obukhov-Corrsin spectrum, as  $E_s = C_{oc} \bar{\chi}_s \bar{\epsilon}^{-1/3} k^{-5/3}$ . However, we stress that the essential quantity characterizing the inertial-convective range dynamics is the scalar transfer flux  $\bar{\Pi}_s$ , as opposed to the mean dissipation rate  $\bar{\chi}_s$ , and they are equal in the steady state. It is this understanding on which we analyze the spectrum [48]. The third term of the r.h.s. of Eq. (86) has the following analytical expression:

$$\int_{k_L}^k F_s(k') dk' = \Lambda_\infty \psi(x), \quad (87)$$

$$\psi(x) = 1 - x + \frac{1}{D_L} \log \left( \frac{\frac{1}{D_L} + x}{\frac{1}{D_L} + 1} \right), \quad (88)$$



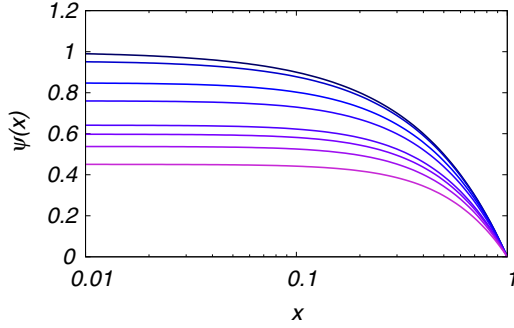


FIG. 7. Variation of  $\psi(x)$  for various Damköhler number and  $x = \text{Da}(k)/D_L$ , where  $k_L$  is the low end of the inertial range. The curves are for  $\text{Da}(k_L) = D_L = 2, 3, 4, 5, 10, 20, 100, \infty$  from the lowest curve.

$$\Lambda_\infty = 2K\Gamma_s^2\bar{\epsilon}\tau_s^2D_L, \quad (89)$$

$$x = \frac{\text{Da}(k)}{D_L} = \left(\frac{k}{k_L}\right)^{-2/3}, \quad 0 < x < 1, \quad (90)$$

where  $D_L = \text{Da}(k_L)$ .  $\psi(x)$  is plotted in Fig. 7 and  $\Lambda_\infty$  corresponds to the maximum supersaturation variance input as  $D_L \rightarrow \infty$ .  $\psi(x)$  indicates the cumulative input of the supersaturation variances from the wave-number range  $k_L$  to  $k$ . Note that  $k_s$  corresponds to  $x_s = \text{Da}(k_s)/D_L = 1/D_L$ . Figure 7 shows, for example, that when  $D_L = 5$  and  $k = k_s$  ( $x_s = 1/5$ ),  $\psi(x_s) \approx 0.6$ , and when  $D_L = 10$  and  $k = k_s$  ( $x_s = 1/10$ ),  $\psi(x_s) \approx 0.75$  are input between  $k_L$  and  $k_s$ . Hereafter we denote  $\psi(x_s) = \psi_s$ .

### 1. Range 1, $k < k_s$

Suppose that  $\text{Da}(k) \gg 1$ . The diffusive effects can be neglected in this range and the relaxation time  $\tau_s$  is much shorter than the turbulence time  $\sigma(k)$ , such that in Eq. (40), the phase relaxation term  $-s/\tau_s$  quickly responds to  $\Gamma_s u_3$  and attains the balance

$$\frac{2}{\tau_s}E_s(k) = A\frac{4}{3}\Gamma_s^2\Theta_F(k)E_u(k), \quad (91)$$

where  $A$  is a proportional constant to be determined via the flux balance given by

$$0 = -\frac{2}{\tau_s} \int_{k_L}^k E_s(k') dk' + \int_{k_L}^k F_s(k') dk'. \quad (92)$$

It is shown in the Appendix that the contributions  $\Pi_s(k)$  and  $\Pi_s(k_L)$  in Eq. (86) arising from the convective term  $T_s(k)$  are negligible when compared to the above two terms. In this approximation, the  $s$  fluctuations are just a footprint of the turbulence, and the spectrum  $E_s(k)$  is thus

$$E_{s1}(k) = \frac{1}{3D_L} \Lambda_\infty \psi_s \bar{\epsilon}^{-1/3} k^{-5/3} \quad \text{for } k < k_s, \quad (93)$$

where  $\psi(x)$  is estimated by  $\psi(x_s)$ , which counts the maximum amount of the input for  $[k_L, k_s]$ .

### 2. Range 2, $k_s < k < k_{s*}$

The wave number  $k_{s*}$  is the transition wave number from  $k^{-5/3}$  to  $k^{-1}$ , as discussed below. We assume that the turbulent eddy time  $\sigma(k)$  is much shorter than  $\tau_s$ , meaning ( $\text{Da}(k) \ll 1$ ), and the term of  $1/\tau_s$  is dropped. The turbulent transfer is fully developed and the triple relaxation time is given by  $\Theta_s(k) = \sigma(k)$ , such that the scalar turbulence prevails. The convective term conserves the

supersaturation variance, and a constant flux is transferred toward high wave numbers throughout this range. Then the Obukhov-Corrsin spectrum (7) is well established with the flux  $\overline{\Pi}_{s2}$  as  $E_{s2}(k) = C_{oc}\overline{\Pi}_{s2}\bar{\epsilon}^{-1/3}k^{-5/3}$ . The flux balance (86) is then given by

$$\begin{aligned}\overline{\Pi}_{s2} \equiv \Pi_s(k) &= -\frac{2}{\tau_s} \int_{k_L}^k E_s(k') dk' + \int_{k_L}^k F_s(k') dk' \\ &= -\frac{2}{\tau_s} \int_{k_L}^{k_s} E_s(k') dk' + \int_{k_L}^{k_s} F_s(k') dk' + \int_{k_s}^k F_s(k') dk' \\ &\approx \Lambda_\infty(1 - \psi_s)\end{aligned}\quad (94)$$

for  $k_s \ll k < k_{s*}$ . The terms of the integrations over  $[k_L, k_s]$  in the second line cancel each other because of Eq. (92), and the contributions of the integral of  $1/\tau_s$  term over  $[k_s, k]$  is dropped by the assumption. The spectrum in this range is thus given by

$$\begin{aligned}E_{s2}(k) &= C_{oc}\overline{\Pi}_{s2}\bar{\epsilon}^{-1/3}k^{-5/3} \\ &= C_{oc}(1 - \psi_s)\Lambda_\infty\bar{\epsilon}^{-1/3}k^{-5/3}.\end{aligned}\quad (95)$$

It is interesting to observe that  $E_{s1}(k)$  and  $E_{s2}(k)$  obey the power law  $k^{-5/3}$  and their ratio is

$$\frac{E_{s2}(k)}{E_{s1}(k)} = 3D_L \frac{1 - \psi_s}{\psi_s}.\quad (96)$$

It should be noted that when  $k_s$  is close to the upper end of the inertial convective range, the Obukhov-Corrsin spectrum Eq. (95) does not exist, because the wave-number range is too narrow for the cascade process to develop.

## B. Strain-convective range

Now consider the spectrum  $E_s^{sc}(k)$  at wave numbers much higher than  $k_{s*}$ . The saturation variance flux  $\overline{\Pi}_{s2}$  in Range 2 is transferred to the high wave numbers without loss according to the 4/3 law. As explained in Sec. II, we substitute the approximate transfer function  $T_s(k)$  into Eq. (79) and obtain

$$\frac{1}{C_B} \left( \frac{\bar{\epsilon}}{\nu} \right)^{1/2} \frac{d}{dk} k E_s^{sc}(k) = -2 \left( \frac{1}{\tau_s} + \kappa_s k^2 \right) E_s^{sc}(k) + F_s(k).\quad (97)$$

The solution is given by the sum of homogeneous and inhomogeneous solutions. The homogeneous solution corresponds to  $\overline{\Pi}_{s2}$ . The inhomogeneous solution to the input  $F_s(k)$  is very small compared to the homogeneous solution because, as seen in Fig. 7,  $\psi(x)$  is almost saturated for  $0.01 < x < 0.05$ , which contributes to Range 2. Thus, the contributions  $d\psi(x)$  for  $x < 0.01$  in this range are negligible. The homogeneous solution is of the form

$$E_s^{sc}(k) = N_s k^{-1} (k\bar{\eta}_{Bs})^{-2C_B D_K} e^{-C_B (k\bar{\eta}_{Bs})^2},\quad (98)$$

where  $\bar{\eta}_{Bs} = Sc_s^{-1/2} \bar{\eta}$  with  $Sc_s = \nu/\kappa_s$  and the constant  $N_s$  is fixed by the normalization

$$\overline{\Pi}_{s2} = 2\kappa_s \int_0^\infty k^2 E_s^{sc}(k) dk.\quad (99)$$

The spectrum is

$$E_s^{sc}(k) = C_B I(\xi) \overline{\Pi}_{s2} \left( \frac{\bar{\epsilon}}{\nu} \right)^{-1/2} k^{-1} (k\bar{\eta}_{Bs})^{-2C_B D_K} e^{-C_B (k\bar{\eta}_{Bs})^2},\quad (100)$$

$$\sim C_B I(\xi) \overline{\Pi}_{s2} \left( \frac{\bar{\epsilon}}{\nu} \right)^{-1/2} k^{-1} (k\bar{\eta}_{Bs})^{-2C_B D_K}, \quad \text{for } k\bar{\eta}_{Bs} \ll 1\quad (101)$$

to the leading order and  $I(\xi)$  is given by

$$I(\xi) = \frac{C_B^\xi}{\Gamma(1 + \xi)}, \quad \xi = C_B D_\kappa, \quad (102)$$

where  $\Gamma(x)$  is the gamma function. For  $k\bar{\eta}_{B\kappa} \ll 1$ , the spectrum is algebraic as  $k^{-1-2C_B D_\kappa}$  and  $I$  tend to unity as  $D_\kappa \rightarrow 0$ .

The transition wave number  $k_{s*}$  is determined by the condition  $E_{s2}(k_{s*}) = E_s^{\text{sc}}(k_{s*})$  and is found to be

$$k_{s*}\bar{\eta} = \left(\frac{C_{\text{OC}}}{C_B}\right)^{3/2} \approx 0.038 \quad (103)$$

for  $D_\kappa \rightarrow 0$ , which is the same as the case of passive scalar Eq. (8).

## VI. SCALING OF LWC SPECTRUM

### A. Inertial-convective range

The analysis proceeds in the same way as before. The transfer function (82) does not contain characteristic time other than the turbulence time  $\sigma(k)$ . Thus, the inertial-convective range is well developed, and  $E_\phi(k)$  follows the Obukhov-Corrsin spectrum with the transfer flux  $\bar{\Pi}_{\phi 1}$  over the range  $[k_L, k_{\phi*}]$ , where  $k_{\phi*}$  is a transition wave number to be determined later at which the spectrum changes from  $k^{-5/3}$  to a shallower spectrum.

The transfer flux is found as follows. Integrating Eq. (80) from  $k_L$  to  $k$  ( $k_L \ll k < k_{\phi*}$ ), we have

$$\begin{aligned} \Pi_{\phi 1}(k) &= 2 \frac{\tau_s}{\tau_l^2} \int_{k_L}^k E_s(k') dk' \\ &= 2 \frac{\tau_s}{\tau_l^2} \left( \int_{k_L}^{k_s} E_{s1}(k') dk' + \int_{k_s}^k E_{s2}(k') dk' \right), \end{aligned} \quad (104)$$

where the diffusion term is dropped. Substituting Eqs. (93) and (95) into Eq. (104), using  $\text{Da}(k_s) = 1$  and noting that the contribution of the second term is negligible compared to the first term for  $k_L \ll k_s \ll k$ , we obtain  $E_{\phi 1}(k)$  as

$$E_{\phi 1}(k) = C_{\text{OC}} \bar{\Pi}_{\phi 1} \bar{\epsilon}^{-1/3} k^{-5/3}, \quad (105)$$

$$\bar{\Pi}_{\phi 1} = \left(\frac{\tau_s}{\tau_l}\right)^2 \Lambda_\infty \psi_s \quad \text{for } k_L < k < k_{\phi*}. \quad (106)$$

Again  $\bar{\Pi}_{\phi 1}$  is constant and consistent with  $E_{\phi 1} \propto k^{-5/3}$ .

### B. Strain-convective range

The 4/3 law for scalar turbulence means that the scalar flux  $\bar{\Pi}_{\phi 1}$  injected in Range 1 is constant until the diffusive effect becomes dominant. In addition to  $\bar{\Pi}_{\phi 1}$ , there exists the additional flux  $\bar{\Pi}_{\phi 2}$  from the source term  $2(\tau_s/\tau_l^2)E_s^{\text{sc}}$ , due to its slow decay in the range  $k\bar{\eta}_{B\kappa} \ll 1$ , as seen in Eq. (101). The equation for  $E_\phi^{\text{sc}}$  in this range is given as

$$\frac{1}{C_B} \left(\frac{\bar{\epsilon}}{\nu}\right)^{1/2} \frac{d}{dk} k E_\phi^{\text{sc}}(k) = -2\kappa_\phi k^2 E_\phi^{\text{sc}}(k) + 2 \frac{\tau_s}{\tau_l^2} E_s^{\text{sc}}(k). \quad (107)$$

The spectrum  $E_{\phi, \text{h}}^{\text{sc}}$  corresponding to  $\bar{\Pi}_{\phi 1}$  that is the homogeneous solution to Eq. (107) is given by

$$E_{\phi, \text{h}}^{\text{sc}}(k) = N_{\phi 1} \bar{\Pi}_{\phi 1} \left(\frac{\bar{\epsilon}}{\nu}\right)^{-1/2} k^{-1} e^{-C_B (k\bar{\zeta}_B)^2}, \quad (108)$$

where  $\bar{\zeta}_B = \text{Sc}_\phi^{-1/2} \bar{\eta}$  with  $\text{Sc}_\phi = \nu/\kappa_\phi$  and the constant  $N_{\phi 1}$  is determined by the normalization condition

$$\bar{\Pi}_{\phi 1} = 2\kappa_\phi \int_0^\infty k^2 E_{\phi, h}^{\text{sc}}(k) dk. \quad (109)$$

We obtain as

$$E_{\phi, h}^{\text{sc}}(k) = C_B \bar{\Pi}_{\phi 1} \left( \frac{\bar{\epsilon}}{\nu} \right)^{-1/2} k^{-1} e^{-C_B (k \bar{\zeta}_B)^2}. \quad (110)$$

Now consider the flux  $\bar{\Pi}_{\phi 2}$  due to the second term of the r.h.s. of Eq. (107). Integrating Eq. (80) from  $k_{\phi*}$  to  $k < k_{\phi d} = 1/\bar{\zeta}_B$  and substituting Eq. (100) into the integral and changing the variables, we have

$$\begin{aligned} \bar{\Pi}_{\phi 2}(k) &= 2 \frac{\tau_s}{\tau_l^2} \int_{k_{\phi*}}^k E_s^{\text{sc}}(k') dk' \\ &= \left( \frac{\tau_s}{\tau_l} \right)^2 I(\xi) \bar{\Pi}_{s2} (k_{\phi*} \bar{\zeta}_B)^{-2C_B D_K}, \end{aligned} \quad (111)$$

for  $k \bar{\zeta}_B \ll 1$ . The spectrum satisfying the normalization condition similar to Eq. (109) [nonhomogeneous solution to Eq. (107)] is

$$E_{\phi, \text{nh}}^{\text{sc}}(k) = C_B \bar{\Pi}_{\phi 2} \left( \frac{\bar{\epsilon}}{\nu} \right)^{-1/2} k^{-1} e^{-C_B (k \bar{\zeta}_B)^2}. \quad (112)$$

Therefore, the spectrum in this range is the sum of two spectra as

$$E_{\phi 2}(k) = C_B \bar{\Pi}_{\phi 1} \left( \frac{\bar{\epsilon}}{\nu} \right)^{-1/2} k^{-1} \left[ 1 + \left( \frac{\tau_s}{\tau_l} \right)^2 I(\xi) \frac{\bar{\Pi}_{s2}}{\bar{\Pi}_{\phi 1}} (k_{\phi*} \bar{\zeta}_B)^{-2C_B D_K} \right] e^{-C_B (k \bar{\zeta}_B)^2} \quad \text{for } k_{\phi*} \ll k. \quad (113)$$

### C. Transition in $E_\phi(k)$

The transition from  $k^{-5/3}$  to the shallower spectrum occurs at the wave number  $k_{\phi*} \bar{\zeta}_B \ll 1$ . The transition wave number  $k_{\phi*}$  in  $E_\phi(k)$  is determined by equating Eq. (105) to Eq. (113), by substituting Eqs. (94) and (106). In the limit of  $k \bar{\zeta}_B \rightarrow 0$ , we obtain

$$C_{\text{oc}} \bar{\Pi}_\phi \bar{\epsilon}^{-1/3} k_{\phi*}^{-5/3} = C_B \bar{\Pi}_\phi \left( \frac{\bar{\epsilon}}{\nu} \right)^{-1/2} k_{\phi*}^{-1} [1 + \gamma (k_{\phi*} \bar{\zeta}_B)^{-2C_B D_K}], \quad (114)$$

$$\gamma = I(\xi) \frac{1 - \psi_s}{\psi_s}. \quad (115)$$

Therefore, the transition wave number  $k_{\phi*}$  is obtained as the solution of the following equation:

$$(k_{\phi*} \bar{\eta})^{2/3} = [1 + \gamma (k_{\phi*} \bar{\eta})^{-2C_B D_K}]^{-1} \left( \frac{C_{\text{oc}}}{C_B} \right), \quad (116)$$

where we set  $\text{Sc}_\phi = 1$  for simplicity so that  $\bar{\zeta}_B = \bar{\eta}$ . When  $D_K \rightarrow 0$ ,  $(k_{\phi*} \bar{\eta})^{-2C_B D_K} \rightarrow 1$ , the above formula simplifies to

$$k_{\phi*} \bar{\eta} = \psi_s^{3/2} \left( \frac{C_{\text{oc}}}{C_B} \right)^{3/2} = \psi_s^{3/2} (k_* \bar{\eta}), \quad (117)$$

where  $k_* \bar{\eta} = (C_{\text{oc}}/C_B)^{3/2}$  is the transition wave number given by Eq. (8). The transition wave number  $k_{\phi*} \bar{\eta}$  changes by the factor  $\psi_s^{3/2}$ , and we obtain  $k_{\phi*} \bar{\eta} < k_* \bar{\eta} \approx 0.038$ , because  $\psi_s < 1$

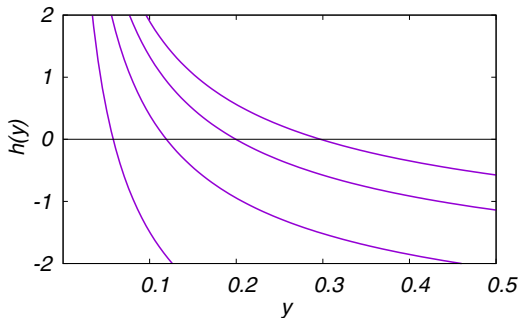


FIG. 8. Zeros of equation  $h(y) = y^{-2/3+2\xi} - y^{2\xi} - a\gamma$ , where  $y = k/k_*$ ,  $a = (k_{\phi_*}\bar{\eta})^{-2\xi} = (C_{Oc}/C_B)^{-3\xi}$ , where,  $\xi = C_B D_\kappa$ . The curves are for  $\psi_s = 0.2, 0.3, 0.4, 0.5$  from the leftmost to the rightmost, respectively.

as shown in Fig. 7. Notably, the correction term depends on the ratio of the total input of the supersaturation fluctuation over Range 2 ( $k_s < k$ ) to the one in Range 1 ( $k < k_s$ ). The smaller the input for  $E_{s1}$  in Range 1 becomes, the bigger the correction is, lowering the transition wave number, which can be restated as the longer the  $\tau_s$  is the bigger the correction becomes.

Let us examine numerically the transition wave number. First, we use the formula Eq. (117). From the data of Siebert *et al.* [6],  $f_c \approx 3$  Hz,  $\bar{\epsilon} = 8.5 \times 10^{-2} \text{ m}^2 \text{ s}^{-3}$ ,  $\nu = 1.33 \times 10^{-5} \text{ m}^2 \text{ s}^{-1}$ ,  $\bar{U} = 4.2$  m/s, and  $u' = 1.4$  m/s, we have  $k_c \bar{\eta} = (2\pi/\bar{U})f_c \bar{\eta} \approx 0.0018$ . As discussed in Sec. III,  $D_L$  is approximately 5; however, here we consider the range of  $D_L = 2-5$ . When we choose  $x_s = \text{Da}(k_s)/D_L = 1/D_L$ ,  $D_L = 2-5$  corresponds to  $x_s \approx 0.5-0.2$ , and  $\psi_s \approx 0.3-0.4$ , as read from Fig. 7. Equation (117) leads to  $k_{\phi_*}\bar{\eta} \approx 0.0062-0.0096$ , which is of the same order as the measurements, but about three times larger than the observed value. As a reference, for smaller values of  $\psi_s = 1/4, 1/5$ , Eq. (116) gives  $k_{\phi_*}\bar{\eta} \approx 0.0048$  and  $0.0034$ , respectively.

Now we apply Eq. (116). The approximate solution is numerically obtained as the zero point of the function  $h(y) = y^{-2/3+2\xi} - y^{2\xi} - a\gamma$ , which is plotted in Fig. 8, where  $y = k/k_*$ ,  $a = (k_*\bar{\eta})^{-2\xi} = (C_{Oc}/C_B)^{-3\xi}$ , and  $\xi = C_B D_\kappa$ , here  $k_*$  is given by Eq. (8). From the data of Ref. [6],  $D_\kappa = 7.0 \times 10^{-3}$  and  $C_B = 6.2$  from the DNS, we estimate  $\xi = 0.04$ . For the four values of  $\psi_s = 0.5, 0.4, 0.3, 0.2$ , the transition wave numbers are  $k_{\phi_*}\eta = 0.012, 0.0078, 0.0047, 0.0023$ , respectively, and the latter two values are close to the observed value. It is interesting to note the transition frequency  $f_*$  corresponding to the above wave numbers. From  $\sigma(k_{\phi_*}) = \bar{\epsilon}^{-1/3} k_{\phi_*}^{-2/3}$ , we obtain the  $f_* = 4.2, 3.3, 2.4, 1.5$  Hz, which is close to the transition frequency shown in Fig. 12 of Siebert *et al.* [6] where the power spectrum deviates from  $f^{-5/3}$  at around  $f_* \approx 2-3$  Hz. On the other hand, the frequency corresponding to the phase relaxation time  $\tau_s = 2-5$  s is about  $0.2-0.5$  Hz, one order smaller than the above estimates, which means that  $k_s < k_{\phi_*}$ .

## VII. DISCUSSION

The supersaturation spectrum has three ranges before the exponential falls off in the diffusive range. In ranges 1 and 2,  $E_s(k)$  is of the power law  $k^{-5/3}$ ; however, the dynamics differs. In the present theory, the variation in the relative importance of the characteristic time  $\tau_s$  and  $\sigma(k)$  is described by the wave-number-dependent Damköhler number  $\text{Da}(k)$  of the triple relaxation time  $\Theta_s$  of transfer function  $T_s(k)$  (see Fig. 5). In Range 1,  $E_{s1}(k)$  is excited at each wave number directly by the velocity component along the uniform mean gradient, due to the short  $\tau_s$ ; the contribution of the convective term is negligible. On the other hand, in Range 2, the excitation at each  $k$  is maintained by the cascade process of the turbulent convection, because the turbulence time  $\sigma(k)$  is shorter than  $\tau_s$ . The change in dynamics occurs at the wave number  $k_s$ , which is determined by  $\text{Da}(k_s) = 1$ . This is the state Mazin argued phenomenologically [8] for the LWC spectrum; however,

here our arguments are not for  $E_\phi(k)$  but for  $E_s(k)$  (see Fig. 6). The ratio  $E_{s2}(k)/E_{s1}(k)$  depends on  $3D_L(1 - \psi_s)/\psi_s$ .

The LWC spectrum in the present theory has a unique  $k^{-5/3}$  power-law scaling range. The supersaturation appears as the driving term in the equation for the logarithm of  $\log q_l$ . If we neglect the  $\kappa_\phi$  term in Eq. (41),  $\phi$  is just the sum of the supersaturation with decorrelation time  $\tau_s$  along the Lagrangian trajectory of the droplet; therefore, the convective term is governed only by the turbulent dynamics, i.e., only  $\sigma(k)$  controls the LWC transfer through the wave-number space. The characteristic time  $\tau_l$  for  $\log q_l$  affects the intensity of excitation by the supersaturation. The effect of the phase relaxation time of the supersaturation is indirect, and the main source of the transfer flux of the LWC variance comes from the Range 1.

The variance fluxes of the supersaturation and LWC cascaded in the inertial-convective range are passed, without loss, in the strain-convective range according to the 4/3 law for the scalar. In the strain-convective range, the spectrum  $E_s^{sc}(k)$  is of the power law  $k^{-1-2C_b D_\kappa}$  that decays slowly as the wave number increases. The LWC spectrum in the strain-convective range has two flows of the variance fluxes: one is from  $\bar{\Pi}_{\phi 1}$  in the inertial-convective range as the cascaded flux, and the other is  $\bar{\Pi}_{s2}$  by the excitation  $E_s^{sc}(k)$ , such that the flux of the LWC variance in this range is augmented by  $(\tau_s/\tau_l)^2 \bar{\Pi}_{s2}$ . This, in turn, leads to the enhancement of  $E_\phi^{sc}$  and makes the transition wave number lower (see Fig. 6).

The explanation for the smaller transition wave number in terms of the enhanced spectrum  $E_\phi^{sc}$  is the same as that given in the study by Jefferey [10]; however, the physical process differs. In [10] the anisotropy of the mean field is considered. In contrast, the chain of excitations, first, the supersaturation excited by the turbulence and, second, the excitation of the LWC by supersaturation through the cascade and direct input, are the main processes responsible for the enhanced level of  $E_\phi^{sc}(k)$  in the present theory. Turbulence has its own timescale depending on the wave number which is not delta correlated. However, the velocity of rapidly changing in time as an approximation corresponds to the relatively infinitely long phase relaxation time, i.e.,  $Da(k) = \sigma(k)/\tau_s \ll 1$ . As discussed in Secs. IV and V, and seen in Fig. 5, the analysis of Jefferey [9–11] with the Batchelor approximation for the strain-convective range cloud be justified in the above sense.

The present analysis suggests that  $E_s(k)$  and  $E_\phi(k)$  are not necessarily the same but may change in different ways; for example, different transition points may exist from  $k^{-5/3}$  to the shallower spectrum or the spectra of the supersaturation, and the LWC is to be measured independently.

Among the assumptions introduced in the present analysis, two assumptions are of note. The first one is that at the scales corresponding to the high end of the inertial-convective range, the turbulence acts as if the rate of strain is effectively uniform. In this case, the Batchelor approximation (16) to the transfer function can be used. Originally, the above approximation was introduced by Batchelor [12] for a large Schmidt number and was theoretically justified only for  $k\bar{\eta} \gg 1$ . However, it has been confirmed numerically that the theoretical prediction  $k_*\bar{\eta} = 0.038$  is in excellent agreement with the DNS data. Unfortunately, we cannot explain these results; however, it is an important problem in the fundamental physics of turbulence and should be investigated further.

The second assumption of note is the neglect of the second-order term in the fluctuations,  $\langle \tilde{q}_l \tilde{s} \rangle$  in Eq. (30) by assuming their smallness. Therefore, the present theory is a linear theory. When the second-order terms are included, it is expected that the interaction between  $\tilde{q}_l$  and  $\tilde{s}$  may generate a spectral transfer from high to low wave numbers. Indeed, in the DNS of the cloud turbulence by Saito and Gotoh [30], their Figs. 8 and 9 show that the enhancement of the water vapor spectrum  $E_q(k, t)$  initially begins in the diffusive range and then propagates toward low wave numbers over time, although it is not certain as to whether the propagation ceases at certain wave numbers. This observation suggests that the inclusion of the second-order term may lead to a further shift of the transition point toward lower wave number.

Finally, we consider the effects of temperature. In the present study, the buoyancy force is neglected so that the scalars, the supersaturation, LWC and temperature are passive. In this situation, the temperature fluctuations is simply the third passive scalar with excitation by the mean uniform gradient  $\Gamma_\theta$  and the supersaturation  $(L_v/c_p \tau_s)s$  in Eq. (42). Therefore, the steady spectrum  $E_\theta(k)$

would be similar to that of  $E_\phi(k)$ , one  $k^{-5/3}$  scaling in the inertial convective range and nearly  $k^{-1}$  scaling in the strain-convective range. The effects of the temperature on the supersaturation and LWC via the constants  $\tau_s$ ,  $\tau_l$ , and  $\Gamma_s$  are indirect and small, we consider that the results remain unchanged in the present setup. When the buoyancy force is included, the physics becomes complicated. However, when the length scales of turbulence under the consideration are smaller than the Bolgiano length  $L_b = \bar{\epsilon}^{5/4} \bar{\chi}_\theta^{-3/4} (g/T_0)^{-3/2}$ ,  $k_s L_b \gg 1$ , it is expected that the scaling of  $E_u(k)$ ,  $E_s(k)$  and  $E_\phi(k)$  is valid [49,50].

### VIII. SUMMARY

We theoretically analyzed the variance spectra of the supersaturation and LWC with the help of DNSs. We showed that the variance spectrum of the scalar, which has its own characteristic time and is carried by the particles without the inertia corresponding to an infinite Schmidt number scalar, has the  $k^{-5/3}$  and  $k^{-1-2C_b D_K}$  power-law ranges. Transition occurs at the wave number  $k_* \bar{\eta} \approx 0.038$ , which is in good agreement with theoretical predictions, in terms of the extended Batchelor approximation for the transfer function of the passive scalar.

The equations for the supersaturation and LWC with continuum expression for the condensation-evaporation rate, which is corpuscular from a microscopic perspective, are derived by coarse graining. The spectral equations of the supersaturation and the LWC variances are derived using the LRA, which is based on Lagrangian dynamics. The spectral equations indicate the chain of the excitations of scalars: first, the excitation of the supersaturation by turbulence, and second supersaturation driving the LWC. The wave-number-dependent Damköhler number determines the transfer of the supersaturation variance in wave-number space. Asymptotic analysis of the transfer flux of the variance of the supersaturation revealed that there exists two  $k^{-5/3}$  ranges in the inertial-convective range depending on whether or not  $Da(k) > 1$ . The crossover of the two ranges occurs at  $k_s$ , defined by  $Da(k_s) = 1$ . The ratio of amplitudes of the two spectra depends on the large-scale Damköhler number and the ratio of the supersaturation inputs in the two ranges. The transition of the supersaturation spectrum from  $k^{-5/3}$  to a shallower spectrum occurs at  $k_* \bar{\eta} = k_{s*} \bar{\eta} \approx 0.038$ .

By applying the same asymptotic analysis to the scalar transfer flux for the LWC variance, we have shown that the LWC spectrum has one  $k^{-5/3}$  power-law range and one shallower spectrum range; they match at the transition wave number  $k_{\phi*}$ , which is a function of the ratio of the supersaturation inputs in the two ranges and is dependent on the product of the Batchelor constant and Damköhler number  $D_K$  corresponding to the Kolmogorov time. Using the observation data measured from the mountain top, we found that the transition wave number in the present theory is close to the observed value.

The present results are based on the asymptotic analysis of the spectral equations so that the computed value of the transition wave number for the LWC spectrum is to be understood qualitatively. However, the physics generating the low-transition wave number for the LWC spectrum are explained as a two-step excitation, consisting of supersaturation driven by turbulence and the LWC excited by supersaturation. For a more precise comparison and deeper understanding, numerical integration of the spectral equations is necessary. The explanation of the success of the Batchelor approximation for the transfer function at much lower wave numbers than the theoretical condition is important and requires closer examination. The extension of the present theory to the nonlinear regime, with the inclusion of the second-order term  $\bar{q}_l \bar{s}$ , is also an important issue. Currently, this work is in progress.

### ACKNOWLEDGMENTS

The work of T.G. was supported by MEXT KAKENHI through Grant No. 20H00225, and JSPS KAKENHI Grants No. 20H02066 for I.S. and No. 18K03925 for T.W. are highly appreciated. High Performance Computing Infrastructure (HPCI, hp200072, hp210056) and Networking, Large-scale Data Analyzing and Information Systems (JHPCN, jh200006, jh210014) are gratefully acknowl-

edged for providing computational resources. The National Institute for Fusion Science, Japan (NIFS18KNSS105, NIFS20KNSS143) is also gratefully acknowledged for supporting computational resources.

### APPENDIX: TRANSFER FLUX IN RANGE 1

Substituting  $U_u(k) = (2\pi)^{-1}K\bar{\epsilon}^{2/3}k^{-11/3}$  and  $U_s = Ak^{-a}$  ( $A > 0, a > 0$ ) into Eq. (81) and using the fact that  $\Theta_S(k) = \tau/2$  and  $\Theta_F(k) = \tau_s$  in this range, we have

$$T_s(k) = 4\pi KA\tau_s\bar{\epsilon}^{2/3}k^{10/3-a}J(a), \quad (\text{A1})$$

$$J(a) = \iint_{\Delta'} d\hat{p} d\hat{q} \hat{p}\hat{q}(1-y^2)\hat{q}^{-11/3}(\hat{p}^{-a}-1), \quad (\text{A2})$$

where  $\hat{p} = p/k$ ,  $\hat{q} = q/k$  and  $\Delta'$  is the domain  $\text{Max}(1-\hat{p}, \hat{p}-1) < \hat{q} < \hat{p}+1$ , and the integral converges and  $J(a)$  is finite. Substituting Eq. (A1) into Eq. (79), we have

$$-4\pi KA\tau_s\bar{\epsilon}^{2/3}J(a)k^{10/3-a} = -E_s(k) + \frac{2}{3}\Gamma_s^2\tau_s^2E_u(k). \quad (\text{A3})$$

Integrating both sides, we obtain an estimate for the flux as

$$4\pi KA\tau_s\bar{\epsilon}^{2/3} \frac{J(a)}{\frac{13}{3}-a} k_L^{13/3-a} = -\int_{k_L}^k E_s(k') dk' + \frac{2}{3}\Gamma_s^2\tau_s^2 \int_{k_L}^k E_u(k') dk'$$

to the leading order. When  $a = 11/3$  and  $k_L \ll k < k_s$ , the left-hand side is  $O(k_L^{2/3})$ , whereas the right-hand-side terms are  $O(k_L^{-2/3})$  such that the contributions from the transfer function are negligible compared to the other two terms.

- 
- [1] A. B. Davis, A. Marshak, H. Gerber, and W. J. Wiscombe, Horizontal structure of marine boundary layer clouds from centimeter to kilometer scales, *J. Geophys. Res.* **104**, 6123 (1999).
  - [2] H. Gerber, J. B. Jensen, A. B. Davis, and A. Marshak, Spectral density of cloud liquid water content at high frequencies, *J. Atmos. Sci.* **58**, 497 (2001).
  - [3] H. Siebert, K. Lehmann, and M. Wendisch, Observations of small-scale turbulence and energy dissipation rates in the cloudy boundary layer, *J. Atmos. Sci.* **63**, 1451 (2006).
  - [4] H. Siebert, R. A. Shaw, and Z. Warhaft, Small-scale velocity fluctuations and internal intermittency in marine stratocumulus clouds, *J. Atmos. Sci.* **67**, 262 (2010).
  - [5] H. Siebert, S. Gerashchenko, A. Gylfason, K. Lehmann, L. R. Collins, R. A. Shaw, and Z. Warhaft, Towards understanding the role of turbulence on droplets in clouds: In situ and laboratory measurements, *Atmos. Res.* **97**, 426 (2010).
  - [6] H. Siebert, R. A. Shaw, J. Ditas, T. Schmeissner, S. P. Malinowski, E. Bodenschatz, and H. Xu, High-resolution measurement of cloud microphysics and turbulence at a mountaintop station, *Atmos. Meas. Tech.* **8**, 3219 (2015).
  - [7] M. Schröder, F. Nordsiek, O. Schlenczek, A. L. Landeta, J. Göttler, G. Bagheri, and E. Bodenschatz, Airborne atmospheric measurements with the Max Planck CloudKites, EGU General Assembly, <https://doi.org/10.5194/egusphere-egu21-11608> (2021).
  - [8] I. Mazin, The effect of condensation and evaporation on turbulence in clouds, *Atmos. Res.* **51**, 171 (1999).
  - [9] C. A. Jeffery, Effect of particle inertia on the viscous-convective subrange, *Phys. Rev. E* **61**, 6578 (2000).
  - [10] C. A. Jeffery, Effect of condensation and evaporation on the viscous-convective subrange, *Phys. Fluids* **13**, 713 (2001).
  - [11] C. A. Jeffery, Investigating the small scale structure of clouds using the  $\delta$  correlated closure: Effect of particle inertia, condensation/evaporation and intermittency, *Atmos. Res.* **59-60**, 199 (2001).



- [12] G. K. Batchelor, Small-scale variation of convected quantities like temperature in turbulent fluid. Part 1. General discussion and the case of small conductivity, *J. Fluid Mech.* **5**, 113 (1959).
- [13] T. Gotoh and P. K. Yeung, Passive scalar transport in turbulence, a computational perspective, in *Ten Chapters in Turbulence*, edited by P. Davidson, Y. Kaneda, and K. R. Sreenivasan (Cambridge University Press, Cambridge, 2013), pp. 87–131.
- [14] T. Gotoh and T. Watanabe, Power and Non-Power Laws of Passive Scalar Moments Convected by Isotropic Turbulence, *Phys. Rev. Lett.* **115**, 114502 (2015).
- [15] R. H. Kraichnan, Small scale structure of a scalar field convected by turbulence, *Phys. Fluids* **11**, 945 (1968).
- [16] R. H. Kraichnan, Convection of a passive scalar by a quasi-uniform random straining field, *J. Fluid Mech.* **64**, 737 (1974).
- [17] R. H. Kraichnan, Anomalous Scaling of a Randomly Advected Passive Scalar, *Phys. Rev. Lett.* **72**, 1016 (1994).
- [18] A. M. Yaglom, Local structure of the temperature field in a turbulent flow, *Dokl. Akad. Nauk. SSSR* **69**, 743 (1949).
- [19] T. Gotoh, T. Watanabe, and Y. Suzuki, Universality and anisotropy in passive scalar fluctuations in turbulence with uniform mean gradient, *J. Turb.* **12**, N48 (2011).
- [20] R. J. Hill, Structure-function equations for scalars, *Phys. Fluids* **14**, 1745 (2002).
- [21] P. K. Yeung, S. Xu, and K. R. Sreenivasan, Schmidt number effects on turbulent transport with uniform mean scalar gradient, *Phys. Fluids* **14**, 4178 (2002).
- [22] D. A. Donzis, K. R. Sreenivasan, and P. K. Yeung, The Batchelor spectrum for mixing of passive scalars in isotropic turbulence, *Flow Turbul. Combust.* **85**, 549 (2010).
- [23] T. Gotoh, T. Watanabe, and H. Miura, Spectrum of passive scalar at very high Schmidt number in turbulence, *Plasma Fusion Res.* **9**, 3401019 (2014).
- [24] K. Iwano, J. Hosoi, Y. Sakai, and Y. Ito, Power spectrum of high Schmidt number scalar in a turbulent jet at a moderate Reynolds number, *Exp. Fluids* **62**, 129 (2021).
- [25] A. M. Obukhov, Structure of the temperature field in a turbulent flow, *Izv. Akad. Nauk. SSSR, Ser. Geogr. Geophys.* **13**, 58 (1949).
- [26] S. Corrsin, On the spectrum of isotropic temperature fluctuations in isotropic turbulence, *J. Appl. Phys.* **22**, 469 (1951).
- [27] A. N. Kolmogorov, Local structure of turbulence in an incompressible fluid at very large Reynolds numbers, *Dokl. Akad. Nauk. SSSR* **30**, 299 (1941).
- [28] G. Falkovich, Bottleneck phenomenon in developed turbulence, *Phys. Fluids* **6**, 1411 (1994).
- [29] I. Saito, T. Gotoh, and T. Watanabe, Spectrum of scalar carried by particles in isotropic turbulence at infinite Schmidt numbers (unpublished).
- [30] I. Saito and T. Gotoh, Turbulence and cloud droplets in cumulus clouds, *New J. Phys.* **20**, 023001 (2018).
- [31] P. A. Vaillancourt, M. K. Yau, and W. W. Grabowski, Microscopic approach to cloud droplet growth by condensation: I. Model description and results without turbulence, *J. Atmos. Sci.* **58**, 1945 (2001).
- [32] P. A. Vaillancourt, M. K. Yau, P. Bartello, and W. W. Grabowski, Microscopic approach to cloud droplet growth by condensation: II. Turbulence, clustering, and condensational growth, *J. Atmos. Sci.* **59**, 3421 (2002).
- [33] C. Siewert, J. Bec, and G. Krstulovic, Statistical steady state in turbulent droplet condensation, *J. Fluid Mech.* **810**, 254 (2017).
- [34] K. K. Chandrakar, I. Saito, F. Yang, W. Cantrell, T. Gotoh, R. A. Shaw, Droplet size distributions in turbulent clouds: Experimental evaluation of theoretical distributions, *Q. J. R. Meteorol. Soc.* **146**, 483 (2019).
- [35] I. Saito, T. Gotoh, and T. Watanabe, Broadening of cloud droplet size distributions by condensation in turbulence, *J. Meteor. Soc. Jpn.* **97**, 867 (2019).
- [36] G. Sardina, F. Picano, L. Brandt, and R. Caballero, Continuous Growth of Droplet Size Variance Due to Condensation in Turbulent Clouds, *Phys. Rev. Lett.* **115**, 184501 (2015).
- [37] A. Celani, G. Falkovich, A. Mazzino, and A. Seminara, Droplet condensation in turbulent flows, *Europhys. Lett.* **70**, 775 (2005).

- [38] A. S. Lanotte, A. Seminara, and F. Toschi, Cloud droplet growth by condensation in homogeneous isotropic turbulence, *J. Atmos. Sci.* **66**, 1685 (2009).
- [39] R. Kubo, M. Toda, and N. Hashitsume, *Statistical Physics II: Nonequilibrium Statistical Mechanics*, 2nd ed. (Springer, New York, 1991).
- [40] T. Ishihara, T. Gotoh, and Y. Kaneda, Study of high-Reynolds number isotropic turbulence by direct numerical simulation, *Annu. Rev. Fluid Mech.* **41**, 165 (2009).
- [41] T. Yasuda, T. Gotoh, T. Watanabe, and I. Saito, Péclet-number dependence of small-scale anisotropy of passive scalar fluctuations under a uniform mean gradient in isotropic turbulence, *J. Fluid Mech.* **898**, A4 (2020).
- [42] Y. Kaneda, Renormalized expansions in the theory of turbulence with the use of the Lagrangian position function, *J. Fluid Mech.* **107**, 131 (1981).
- [43] Y. Kaneda, Inertial range structure of turbulent velocity and scalar fields in a Lagrangian renormalized approximation, *Phys. Fluids* **29**, 701 (1986).
- [44] T. Gotoh, J. Nakagi, and Y. Kaneda, Passive scalar spectrum in the viscous-convective range in two-dimensional steady turbulence, *Phys. Fluids* **12**, 155 (2000).
- [45] T. Gotoh, R. S. Rogallo, J. R. Herring, and R. H. Kraichnan, Lagrangian velocity correlations in homogeneous isotropic turbulence, *Phys. Fluids A* **5**, 2846 (1993).
- [46] Y. Zhou, Turbulence theories and statistical closure approaches, *Phys. Rep.* **935**, 1 (2021).
- [47] W. J. T. Bos, On the anisotropy of the turbulent passive scalar in the presence of a mean scalar gradient, *J. Fluid Mech.* **744**, 38 (2021).
- [48] R. H. Kraichnan, On Kolmogorov's inertial-range theories, *J. Fluid Mech.* **62**, 305 (1974).
- [49] R. Bolgiano, Turbulent spectra in a stably stratified atmosphere, *J. Geophys. Res.* **64**, 2226 (1959).
- [50] A. S. Monin and A. M. Yaglom, *Statistical Fluid Mechanics*, Vol. 2 (MIT Press, Cambridge, MA, 1975).